JCI insight

Targeting gliovascular connexins prevents inflammatory blood-brain barrier leakage and astrogliosis

Marijke De Bock, … , Roosmarijn E. Vandenbroucke, Luc Leybaert

JCI Insight. 2022. https://doi.org/10.1172/jci.insight.135263.

Research In-Press Preview Inflammation Neuroscience

Graphical abstract

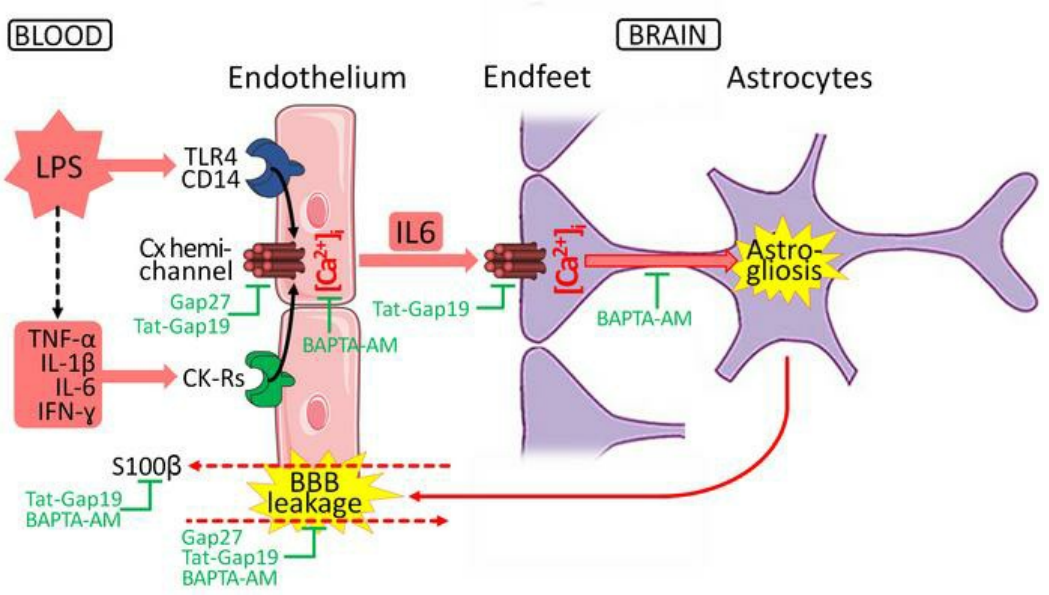

Targeting gliovascular connexins prevents inflammatory blood-brain barrier leakage and astrogliosis

Marijke De Bock[1§], Maarten De Smet[1§], Stijn Verwaerde[1], Hanane Tahiri[1], Steffi Schumacher[1], Valérie Van Haver[1], Katja Witschas[1], Christian Steinhäuser[2], Nathalie Rouach[3], Roosmarijn E. Vandenbroucke[4] and Luc Leybaert[1]

§ are co-first authors

[1]Physiology group, Department of Basic and Applied Medical Sciences, Ghent University, Ghent, Belgium

[2]Institute of Cellular Neurosciences, University of Bonn, Medical School, Bonn, Germany

[3]Center for Interdisciplinary Research in Biology, College de France, CNRS, Inserm, Université PSL, Paris, France

[4]Department of Biomedical Molecular Biology, Ghent University and Inflammation Research Center, VIB, Ghent, Belgium

The authors have declared that no conflict of interest exists.

Address correspondence to: Luc Leybaert, Department of Basic and Applied Medical Sciences - Physiology group, Faculty of Medicine and Health Sciences, Ghent University, C. Heymanslaan 10, Block B (entrance 36) - 3rd floor, 9000 Ghent, Belgium; Tel: +32.9.332.33.66, E-mail: luc.Leybaert@UGent.be. ORCID ID: 0000-0001-6452-6982

Abstract

The blood-brain barrier is formed by capillary endothelial cells expressing Cx37, Cx40 and Cx43, and is joined by closely apposed astrocytes expressing Cx43 and Cx30. We investigated whether connexin-targeting peptides could limit barrier leakage triggered by LPS-induced systemic inflammation in mice. Intraperitoneal LPS increased endothelial and astrocytic Cx43 expression, elevated TNFα, IL1β, IFNγ and IL6 in plasma and IL6 in the brain, and induced barrier leakage recorded over 24h. Barrier leakage was largely prevented by global Cx43 knockdown and Cx43/Cx30 double-knockout in astrocytes, slightly diminished by endothelial Cx43 knockout and not protected by global Cx30 knockout. Intravenous administration of Gap27 or Tat-Gap19 just before LPS also prevented barrier leakage, and intravenous BAPTA-AM to chelate intracellular calcium was equally effective. Patch-clamp experiments demonstrated LPS-induced Cx43 hemichannel opening in endothelial cells, which was suppressed by Gap27, Gap19 and BAPTA. LPS additionally triggered astrogliosis that was prevented by intravenous Tat-Gap19 or BAPTA-AM. Cortically applied Tat-Gap19 or BAPTA-AM to primarily target astrocytes, also strongly diminished barrier leakage. *In vivo* dye uptake and *in vitro* patch-clamp showed Cx43 hemichannel opening in astrocytes that was induced by IL6 in a calcium-dependent manner. We conclude that targeting endothelial and astrocytic connexins is a powerful approach to limit barrier failure and astrogliosis.

Introduction

Efficient neuronal signaling in the central nervous system (CNS) strictly depends on a balanced and well-controlled microenvironment around glial cells, synapses and axons. This is achieved by a series of physical barriers interposed between the nervous tissue, the blood and the cerebrospinal fluid, that collectively protect the brain from fluctuations in blood and CSF composition. The most stringent barrier is the blood-brain barrier (BBB) that is formed by an extremely dense network of capillary endothelial cells (ECs) that separate the brain from the blood in such a way that almost every neuron has a local barrier interface in its microenvironment. Unique features of brain capillary ECs are responsible for the BBB's restrictive function. These include a complex belt of tight junctions (TJs) and adherens junctions sealing off the paracellular cleft, the presence of a thick continuous glycocalyx, severely reduced non-specific vesicular activity, and a strictly regulated set of transporters that controls near-to-all passage in and out of the brain. Endothelial barrier properties are furthermore controlled by surrounding partner cells, including astrocytes and pericytes (1). Among these, astrocytes have been best characterized for their influence on BBB function. Their endfeet projections nearly completely surround the capillary endothelium and exert a trophic influence on the BBB that has been well-characterized in terms of CNS development and a plethora of astrocyte-secreted molecules that maintain expression of junctional proteins, transporters and other barrier features in brain capillaries (2). Astrocytes respond to all forms of brain injury and disease through the process of astrogliosis, thereby producing neurotrophic factors, growth factors, cytokines, chemokines, neurotransmitters, reactive oxygen species, and proteases that may detrimentally affect BBB function (2-4). Astrocytic endfeet are closely appositioned to capillary endothelial cells but separated from the latter by a basal lamina. Several connexins are expressed at this gliovascular interface, including endothelial Cx37, Cx40 and Cx43, and astrocytic Cx43 and Cx30 (5, 6) that have established channel roles in each cell type but do not interconnect astrocytes with endothelial cells by gap junctions (7). Astrocytic endfeet are known to play a role in the communication of calcium (Ca^{2+}) signals alongside the vessel wall and in the process of neurovascular coupling (7-10); however, fairly little is known on their contribution to endothelial barrier function. Astrocytic deletion of Cx30 and Cx43 has no effect on baseline

barrier permeability but renders it more vulnerable to increased hydrostatic pressure (6). Moreover, absence of astrocytic Cx43 promotes endothelial immune activation, allowing the infiltration of lymphocytes, macrophages and neutrophils (11). Here, we investigated the contribution of endothelial and astrocytic Cx43 to BBB alterations induced by systemically administered lipopolysaccharide (LPS), a Gram-negative bacterial wall component that triggers an innate immune response through activation of Toll-like receptor 4 and CD14 (12-14). We used two different approaches to target endothelial cells and astrocytes, by applying inhibitors of connexin channel function and intracellular Ca^{2+} dynamics either intravenously (IV) or directly at the exposed brain cortex where cell-permeating molecules have access to astrocytes via the glia limitans. We found that IV administered barrier-impermeable Gap27 strongly protects against barrier leakage, while barrier-permeable Tat-Gap19 protected against barrier leakage and astrogliosis. Tat-Gap19 also strongly inhibited barrier leakage when applied to the cortical surface. Overall, barrier-protection was not clearly linked to astrogliosis or to LPS-induced alterations in pro-inflammatory cytokines in blood and brain. Instead, barrier-protection was linked to inhibition of Ca^{2+}-dependent Cx43 hemichannel activation in endothelial cells and astrocytes, with brain IL6 functioning as a hemichannel activator in astrocytes.

Results

Intraperitoneal injection of LPS induces systemic and cerebral inflammation along with barrier leakage

We tested various LPS doses (1-50 mg/kg IP) and found 100 % mouse survival up to 25 mg/kg in the 24 h experimental observation window (**Fig. 1A**). Next, we verified the effect of the various LPS doses on barrier permeability, determined by the leakage of IV-injected 3 kDa dextran-fluorescein (DF) into the brain (30 mg/kg, 10 min prior to sacrifice and brain isolation). Twenty-four hours after LPS, significant tracer leakage in the cerebral cortex was observed with 5 mg/kg LPS or higher, approaching a plateau at 25 mg/kg (**Fig. 1B**). We chose the 25 mg/kg sub-maximal concentration for optimal signal stability compared to half-maximal effect concentration where small concentration changes produce large changes in leakage effect. To document LPS-induced barrier leakage for a range of distinct molecular weight tracers, we included 10 kDa DTR and 66 kDa FITC-albumin and found leakage for the 3 and 10 kDa dextran tracers but not for the 66 kDa tracer, indicating barrier function was still intact for albumin (**Fig. 1C**). To characterize peripheral inflammation, we analyzed plasma levels of the pro-inflammatory cytokines IL1β, TNFα, IFNγ and IL6 and found that all but IFNγ were significantly increased at the earliest (3 h) time point, followed by a decline towards the end of the recording (**Fig. 1D**), as observed in rodents treated with lower LPS doses (15, 16). IFNγ showed a delayed response and increased at 6 and 24 h after LPS injection. In the brain, IL1β and TNFα levels did not significantly change over the 24 h window and IFNγ levels fell below the assay's detection limit, notwithstanding their strong peripheral levels. By contrast, brain IL6 levels reliably followed the time course of plasma IL6, peaking at 3 and 6 h post-LPS and declining thereafter (**Fig. 1E**).

LPS triggers increased Cx43 expression in barrier endothelial cells and astrocytes

Although the role of BBB endothelial Cx43 is far less characterized than it is for glial cells, accumulating evidence suggests its involvement in barrier leakage (5). *In vivo*, Cx43 expression is low in brain microvascular endothelium, but increases after pathological insults such as ischemia, trauma and cerebral cavernous malformations (17-19). Here, we found increased Cx43 expression in primary cultures of mouse brain capillary endothelial cells (BCECs) exposed

to LPS (1 μg/mL) *in vitro* (**Fig. 2A**), as well as in intact brain capillaries isolated from mice treated with LPS (25 mg/kg) (**Fig. 2B-C**). Staining of isolated brain capillaries with the endothelial marker CD31 and the astrocytic endfeet marker AQP4 allowed to distinguish Cx43 expression in these two cell types. Cx43 changes in astrocytic endfeet are shown in **Fig. 2D-E**, demonstrating a significant increase at 6 h while significance was attained at 3 h for capillary endothelial cells (**Fig. 2C**). We also tested the effect of LPS treatment on endothelial Cx37 and Cx40, and found those to be lowered 24 h after LPS administration, however, without attaining statistical significance (**Fig. S1**).

LPS-induced barrier leakage is inhibited by intravenously administered connexin-targeting peptides and intracellular Ca^{2+} chelator BAPTA-AM

To investigate the role of Cx43 in BBB leakage *in vivo*, Gap27 and Tat-Gap19 peptides were administered IV immediately (<1 min) before challenging the animals with IP-injected LPS. Gap27 targets an extracellular domain in the Cx43 protein sequence and acts from the outside, inhibiting hemichannels within minutes and gap junctions within hours (20-23). Tat-Gap19 binds to the intracellular C-terminal tail of Cx43 and inhibits hemichannels within minutes while not inhibiting gap junctions (reviewed in (24)). It crosses the BBB and reaches the astrocytes where it associates with Cx43 (25, 26). We found that a single IV injection of Gap27 or Tat-Gap19 potently inhibited LPS-induced BBB leakage over the entire 24 h observation window. Control experiments with scrambled Gap27 and Tat peptide not fused to Gap19 showed no effect on LPS-induced BBB leakage (**Fig. 3A**). Intravenous Gap27 had no significant effects on plasma IL1β, TNFα, IFNγ and IL6 and brain IL6; Tat-Gap19 suppressed the 3 h plasma TNFα increase and enhanced the 6 h brain IL6 elevation (**Fig. S2**). As the Tat-Gap19 effects were not consistent (suppressing TNFα, enhancing IL6), peptide inhibition of barrier leakage is unlikely to result from altered inflammatory processes at the blood or brain side.

Connexin channels are intimately linked to $[Ca^{2+}]_i$ signaling in BBB endothelial cells (22, 27), and we further determined the role of Ca^{2+} in LPS-induced barrier leakage making use of *in vivo* intracellular Ca^{2+} chelation with cell-permeant BAPTA-AM. Such approach has been shown to reduce infarct volume in mouse focal cerebral ischemia (28) and to improve spatial learning in

aged rats (29). Control experiments demonstrated that IV BAPTA-AM (12 mg/kg, 30 min before LPS) did not affect animal survival that remained at 100 % for BAPTA-AM and for the DMSO vehicle (n = 8, data not shown). In terms of barrier function, IV BAPTA-AM treatment potently inhibited LPS-induced leakage of 3 kDa DF and 10 kDa DTR (**Fig. 3B**). BAPTA-AM did not affect IL1β, TNFα and IFNγ but delayed the IL6 elevation in the brain (compare **Fig. S3** to Fig. 1D-E).

To determine whether prevention of BBB leakage by the peptide/BAPTA-AM treatments applied, involved alterations int the tight junction proteins, we verified the effect of these experimental conditions on the expression of occludin and claudin in primary BCECs. Neither LPS alone, nor its combination with Gap27 or Tat-Gap19 treatments had any effect on the expression levels of occludin or claudin **(Fig. S4)**. BAPTA-AM showed a tendency to decrease claudin expression; however this compound efficiently protected against LPS-triggered BBB leakage, bringing us to the conclusion that the observed claudin changes do not play any role in the protective effect of BAPTA-AM.

LPS-induced barrier leakage is strongly reduced by inducible global Cx43 knockdown and Cx43/Cx30 double knockout in astrocytes

We used different Cx43 knockout mouse lines to further substantiate the importance of Cx43 in LPS-induced barrier leakage. Tamoxifen-induced global Cx43 knockdown in $Cx43^{Cre\text{-}ER(T)}/C43^{Fl}$ mice, exhibiting a 65 ± 5.0 % (n = 3; measured in heart) reduction in Cx43 after tamoxifen treatment, were entirely protected against LPS-induced barrier leakage for 3 and 10 kDa tracers at all time points (**Fig. 4A**).

For astrocytes, we used mice with conditional astrocytic Cx43 deletion under control of the GFAP promotor (GFAP-Cre/$Cx43^{fl/fl}$) combined with global Cx30 knockout to prevent compensatory astrocytic Cx30 upregulation, further referred to as astrocytic Cx43/Cx30 double knockout mice (30, 31). These double knockout animals, displaying a 48 ± 7 % (n = 3) reduction of astrocytic Cx43 expression (**Fig. S5A**), were protected against LPS-induced barrier leakage (**Fig. 4B**). By contrast, Cx30 knockout mice still displayed leaky barriers 6 h after LPS administration, as WT mice (**Fig. 4B**). Baseline BBB function was normal in these animals (3 kDa

tracer leakage in WT: 20347 ± 9265 a.u.; $Cx30^{KO}$: 22337 ± 9109 a.u.; $Cx30^{KO}$:GFAP-Cre^{NEG}: 29629 ± 7331 a.u.; $Cx30^{KO}$:GFAP-Cre^{POS} littermates: 31692 ± 5681 a.u.; n = 3-5), as reported by others (6, 32); under high pressure conditions leakage may however occur (6, 33).

Conditional endothelial Cx43 knockout mice were obtained by crossing mice carrying loxP sites flanking exon 2 of the Cx43 gene ($Cx43^{fl/fl}$ mice) with mice expressing Cre under control of the Tie-2 promoter. Western blotting studies demonstrated a 64 ± 4 % (n = 5) reduction of Cx43 expression in BCECs isolated from Cx43fl:Tie2-Cre^{POS} mice relative to Cx43fl:Tie2-Cre^{NEG} control mice (**Fig. S5B**). LPS-induced barrier leakage tended to be decreased in Cx43fl:Tie2-Cre^{POS} mice (Fig. 4C) but the effect did not attain statistical significance when compared to Cx43fl:Tie2-Cre^{NEG} animals. Possibly, this may relate to an observed upregulation of Cx37 expression in primary BCECs from Cx43fl:Tie2-Cre^{POS} animals (196 ± 83.9 %; n = 3; p = 0.024).

LPS triggers rapid endothelial hemichannel opening that is suppressed by Gap27, Gap19 and intracellular Ca^{2+} chelation

The fact that a single IV injection of the rapidly cleared hemichannel-inhibiting Tat-Gap19 peptide (~17.5 min half-life in the blood, calculated as described in Mathur et al., 2018 (34)) prevented barrier leakage up to 24 h later, indicates that early hemichannel opening may be crucial in the event cascade. We thus determined whether LPS could directly stimulate Cx43 hemichannel opening in addition to its activation by TNFα and IL1β that has been characterized previously (35, 36). We made use of patch-clamp experiments on HeLa cells overexpressing Cx43 (HeLaCx43) and on RBE4 cells derived from rat brain endothelium. In HeLaCx43 cells, voltage steps to +70 mV activated unitary current activity characterized by a unitary conductance (γ) of ~220 pS corresponding to hemichannel opening (**Fig. S6A**). Within 120 s after LPS (1 µg/mL, applied via a fast local perfusion system), unitary current activity significantly increased, resulting in a doubling of membrane charge transfer (Q_m) compared to baseline (**Fig. S6B**). Quantification of tail current hemichannel closing events upon repolarization (see dashed boxes in **Fig. S6A**) confirmed a rapid increase in hemichannel activity with LPS (**Fig. S7A**). LPS-enhanced hemichannel activity rapidly reverted to baseline within 40 s after washout (**Fig. S6B**). Control experiments without LPS challenging or with LPS challenging of wild-type HeLa cells not

overexpressing Cx43 had no effect (**Fig. S6D** and **Fig. S7C-D**). Gap19 (applied via the whole-cell patch pipette and therefore without Tat-internalization sequence) and Gap27 (bath solution) strongly inhibited the LPS-enhanced hemichannel opening (**Fig. S6C-D and E-F** and **Fig. S7D and F-G**). LPS also rapidly triggered $[Ca^{2+}]_i$ transients in HeLaCx43 cells (**Fig. S7E**) and to test whether $[Ca^{2+}]_i$ signaling played a role stimulating hemichannel opening, we loaded the cells with BAPTA (10 mM, added via the patch pipette) and found it to strongly inhibit LPS-enhanced hemichannel activity (**Fig. S6C-D** and **Fig. S7D**).

We next verified LPS effects in RBE4 cells aiming to determine whether this could activate Cx43 hemichannel opening at normal negative resting potential. As observed in HeLaCx43 cells, LPS rapidly triggered $[Ca^{2+}]_i$ changes that were oscillatory in ~1/3 of the cells (**Fig. 5A-C**). These $[Ca^{2+}]_i$ responses were inhibited by Gap27 and Tat-Gap19 indicating they are related to hemichannel opening (**Fig. 5B-C**). Addition of a mix of cytokines (TNFα, IL1β, IL6, IFNγ) that were elevated in the blood after LPS (Fig. 1D) also triggered $[Ca^{2+}]_i$ responses that were oscillatory in ~2/3 of the cells (**Fig. 5D-F**). We subsequently tested whether hemichannel activity could be provoked by electrical stimulation over the -60 to +60 mV range and verified the effect of 50 and 250 nM $[Ca^{2+}]_i$ (imposed through the patch pipette). In the 50 nM $[Ca^{2+}]_i$ control condition, unitary current activities only appeared at +60 mV; at 250 nM $[Ca^{2+}]_i$, unitary current activity also appeared at negative membrane potential while currents at positive potential were enhanced (**Fig. 6A**). An I–V plot of current amplitudes indicated a slope conductance of 228 ± 1 pS, typical for Cx43 hemichannels (**Fig. 6B**). Gap19 and Gap27 potently inhibited unitary currents at both negative and positive potentials (**Fig. 6A**). All-point histograms of unitary current activities at -60 mV and +60 mV (**Fig. 6C**) indicated a single-channel conductance in the range of the slope conductance obtained from the I–V plot. Fig. 6C summarizes Q_m data demonstrating 250 nM Ca^{2+}-stimulation of hemichannel activity as well as Gap27/Gap19 inhibition for negative and positive potentials. We further tested whether LPS could directly trigger hemichannel opening under low $[Ca^{2+}]_i$ buffering conditions (0.1 mM EGTA in patch pipette instead of 2 mM) and with the cells held at -50 mV. Most interestingly, we found that LPS (1 µg/mL) triggered current activity with a ~210 pS unitary conductance and ~60 pS substate characteristic of Cx43 hemichannels (**Fig. 6D-E**); extracellular solution without LPS had no effect

(**Fig. 6D**, vehicle control). Gap19, Gap27 and intracellular BAPTA (10 mM in the pipette) all abolished the LPS-induced hemichannel currents (**Fig. 6D, F**).

LPS induces astrogliosis that is prevented by Tat-Gap19 and BAPTA-AM

Intraperitoneally administered LPS and the associated systemic cytokine surge will first activate the BBB endothelium, but astrocytes will subsequently become involved and may, as reactive astrocytes, further impair barrier function. Reactive astrocytes display increased GFAP gene expression (37) and immunohistochemical analysis confirmed significantly elevated GFAP signal starting from 6 h post-LPS and persisting up to 24 h (**Fig. 7A-B**). Treatment with IV-administered BAPTA-AM and Tat-Gap19 prevented the GFAP increase while the less permeable Gap27 had no effect (**Fig. 7B**). Tat-Gap19 enhanced the 6 h brain IL6 elevation (**Fig. S2B**) and prevention of GFAP elevation by Tat-Gap19 does therefore not seem to link to IL6. S100β, an 11 kDa soluble Ca^{2+}-binding protein, is another astrogliosis marker that is released from astrocytes in inflammation-linked brain disorders (38-40), as well as by LPS (41), pro-inflammatory cytokines (42, 43) and elevated $[Ca^{2+}]_i$ (44). We found significantly increased S100β levels in the plasma starting at 6 h post-LPS and increasing to the 24 h time point (**Fig. 7C-D**). As observed for GFAP, S100β appearance in the plasma was inhibited by Tat-Gap19 but not by Gap27; in contrast to GFAP, IV BAPTA-AM had no effect (**Fig. 7D**).

BAPTA-AM and Tat-Gap19 applied directly to the cortical surface via a cranial window prevent barrier leakage

To further identify the role of brain parenchymal $[Ca^{2+}]_i$ changes and astrocytic Cx43 hemichannels in BBB leakage, we performed experiments with BAPTA-AM and Tat-Gap19 directly applied to the exposed cerebral cortex (**Fig. 8A**). Application of the fluorescent indicator sulforhodamine 101 (SR101) via a cranial window has been demonstrated to be taken up specifically by astrocytes (45, 46) and AM ester-based Ca^{2+} indicator loading via this way is an established procedure for monitoring astrocytic $[Ca^{2+}]_i$ dynamics (47-49). Here, we applied BAPTA-AM via the exposed cortex to determine whether astrocytic Ca^{2+} chelation could

mitigate barrier leakage induced by IP-administered LPS. Cortical barrier leakage was quantified in the SR101-positive zone (**Fig. 8A**). BAPTA-AM significantly prevented LPS-induced BBB leakage of 3 kDa DF (**Fig. 8B**) while it had no effect in non-LPS treated control animals (BAPTA-AM: 32178 ± 6554 a.u.; vehicle: 21020 ± 3998 a.u.; n = 3, non-significant). Cranial window application of Tat-Gap19 also strongly protected against LPS-induced barrier leakage (**Fig. 8C**), while it had no effect in non-LPS treated control animals (Tat-Gap19: 33242 ± 6443 a.u.; vehicle: 27670 ± 1918 a.u.; n = 3).

LPS triggers astroglial Cx43 hemichannel opening mediated by IL6

To assess cortical Cx43 hemichannel opening in response to IP-administered LPS, we made use of dye uptake studies whereby hemichannel-permeable EtBr was applied *in vivo* on the exposed cortex followed by subsequent counting of EtBr-positive cells in isolated cortical cryosections. We observed a sharp increase in the number of dye positive cells at 6 and 24 h after LPS injection (**Fig. 9A-B**). The number of dye positive cells was significantly reduced to baseline when Tat-Gap19 was included in the EtBr solution applied to the exposed cortex (30 min 200 µM Tat-Gap19 that was continued in the presence of 100 µM EtBr for the next 30 min) (**Fig. 9C**).

LPS is known to indirectly trigger astrocytic hemichannel opening via activation of microglial cells that release TNFα and IL1β (35, 50, 51). However, systemically administered LPS is not likely to enter the brain (Banks and Robinson, 2010) nor did we find elevated brain TNFα and IL1β levels in response to systemic LPS (Fig. 1E). More interestingly, we found increased brain IL6 levels (Fig. 1E), the effect of which on Cx43 hemichannels is currently unknown. We thus explored IL6 effects on hemichannel currents in HeLaCx43 cells and primary cultured cortical astrocytes. Hemichannel currents in HeLaCx43 cells were significantly enhanced by 100 ng/mL IL6 within 80 seconds (~2-fold increase in Q_m and hemichannel closing event counts) and reverted to baseline within 40 s after washout (**Fig. 10A-B** and **Fig. S8**). Gap19 and BAPTA strongly inhibited these responses (**Fig. 10C-D** and **Fig. S8D**). Cx43 hemichannel opening can be directly activated by $[Ca^{2+}]_i$ in astrocytes (26, 52) and we here found IL6-induced $[Ca^{2+}]_i$ changes to be inhibited by Tat-Gap19, indicating a linkage to hemichannel opening (**Fig. 10F**). We thus

performed patch-clamp experiments on primary cultured astrocytes held at -70 mV under low intracellular Ca^{2+} buffering conditions (0.1 mM EGTA in patch pipette) and exposed them to IL6 (100 ng/mL), which induced unitary current activities with a conductance as expected for Cx43 hemichannels (**Fig. 10E,G**). Gap19 and BAPTA significantly inhibited these responses, demonstrating Ca^{2+}-dependent hemichannel activation (**Fig. 10E,H**).

Discussion

LPS is a frequently used experimental tool to initiate a systemic inflammatory response that spreads out to the cerebral parenchyma. LPS itself poorly penetrates into the brain (53, 54) (**Fig. 11** ①), but exerts its cerebral effects via an innate immune response through activation of endothelial Toll-like receptor 4 and CD14 (12-14) (**Fig. 11** ②). Additionally, LPS triggers a cytokine storm with IL1β, TNFα, IL6 and IFNγ as major proponents (55, 56) (**Fig. 11** ③) that disturb BBB function (57-59) (**Fig. 11** ④). We here provide evidence that LPS and circulating cytokines increase the low baseline Cx43 expression in the barrier endothelium and its high baseline expression in astrocytic endfeet. LPS/cytokines furthermore activate $[Ca^{2+}]_i$ dynamics and hemichannel opening (**Fig. 11** ⑤). Cx43 hemichannels have been demonstrated to sustain $[Ca^{2+}]_i$ oscillations and thereby contribute to barrier leakage (22, 60), so barrier leakage likely results from endothelial LPS/cytokine effects combined with hemichannel opening (**Fig. 11** ⑥). *In vivo* interfering with connexins and $[Ca^{2+}]_i$ by IV administration of Gap27, Tat-Gap19 or BAPTA-AM (marked red in **Fig. 11**) prevents the LPS-induced barrier failure.

In addition to their barrier forming role, BBB endothelial cells are also a relay station in immune-brain communication by secreting immune factors and pro-inflammatory cytokines, in particular IL6 as reported here. Possibly, circulating IL6 (MW 21 kDa) may have leaked through the barrier, as suggested by the synchronized IL6 peaks at 3 and 6h in plasma and brain (Fig. 1 D&E). However, one would then expect leakage of other cytokines, with MW in the order of the 3 and 10 kDa fluorescent leakage markers used (IL1β 1 kDa, IFNγ ~17 kDa), to also appear in the brain, which was not the case. The fact that IL6 was the only cytokine (out of 4 tested) elevated in the brain indicates that more specific mechanisms are involved. IL6 exerts its effects via a receptor complex that consists of the IL6 receptor (IL6R) and the signal transduction receptor subunit gp130 (61, 62). Both gp130 and IL6R are widely distributed throughout the brain and are upregulated by exposure to pro-inflammatory conditions (63, 64). IL6 receptors are present in astrocytic endfeet (65) and their activation may induce reactive astrocytosis (astrogliosis) (66, 67). We here demonstrate that IL6 triggers astrocytic $[Ca^{2+}]_i$ dynamics as well as Cx43 hemichannel opening (**Fig. 11** ⑦). $[Ca^{2+}]_i$ changes interact with hemichannels in a bimodal

manner (68), sustaining astrocytic $[Ca^{2+}]_i$ dynamics (22, 60) and thereby leading to astrogliosis (**Fig. 11** ⑧). Reactive astrocytes on their turn upregulate pro-inflammatory and cytotoxic pathways, and consequently produce a range of substances associated with barrier leakage (61, 69, 70); reviewed in (67) (**Fig. 11** ⑨). In line with this event sequence, IV administration of barrier-permeable BAPTA-AM and Tat-Gap19, prevent GFAP upregulation, which is supported by *in vitro* evidence for a role of astrocytic $[Ca^{2+}]_i$ therein (71-73).

Common vasodilatory agents that are released from astrocytic endfeet in a Ca^{2+}-dependent manner during neurovascular coupling such as e.g. adenosine and prostaglandin E2 (74, 75); reviewed in (76)), have also known BBB-disintegrating effects and may contribute to barrier leakage (77-82) (**Fig. 11** ⑩). Last but not least, cortically applied Tat-Gap19 and BAPTA-AM aimed at targeting astrocytes potently inhibited barrier leakage, supporting a forefront role of astrocytic Cx43 hemichannels and $[Ca^{2+}]_i$ signaling in barrier leakage in response to peripheral inflammation.

Intravenous BAPTA-AM strongly protected against BBB leakage, most likely by its first-line actions in the vascular compartment and its diffusion to subsequent cell layers, including astrocytes. Neurons also take up BAPTA-AM (28, 83) but ester-loading is in general less efficient than in astrocytes (84). The fact that IV BAPTA-AM potently prevented GFAP upregulation in astrocytes (**Fig. 8B**) indicates excellent astrocytic BAPTA-loading and tempering of $[Ca^{2+}]_i$ dynamics, thereby contributing to barrier-protection as demonstrated by the cranial window BAPTA-AM applications that showed equally strong protection as observed with IV injection. Tat-Gap19 has an intracellular target, the C-terminal tail of Cx43 (85), and is BBB permeable. One hour after systemic administration, it is detected in GFAP-positive astrocytes where it co-localizes with Cx43 and is still detectable in the parenchyma after 24 h (25, 26). Moreover, systemically administered Tat-Gap19 has been shown to decrease seizure activity in animal epilepsy models (86) and to prevent neuronal cell loss in Parkinson's disease (87), indicating it is biologically active in the brain. In contrast, Gap27 has an extracellular target (extracellular loops of Cx43 and Cx37) and has no known intrinsic membrane permeability, making its entry into the

barrier-intact brain unlikely. Given the short lifetime of Gap27 circulating in the blood (~14 min half-life), it is highly unlikely that the barrier would be sufficiently leaky to allow significant peptide entry into the brain. Thus, we anticipate that IV Gap27 prevents BBB leakage by inhibiting connexin channels in the luminal endothelial membranes, whereas IV Tat-Gap19 will target Cx43 hemichannels in both endothelial cells and astrocytes. IV Gap27 had an overall stronger effect against barrier leakage compared to IV Tat-Gap19, which may result from Gap27 affecting connexins other than Cx43, e.g. endothelial Cx37 that has the same EL2-located peptide sequence as for Cx43, or potential inhibition of gap junctions, an effect not exerted by Tat-Gap19. However, gap junctional inhibition by Gap27 necessitates more than 6 h, i.e. far beyond its ~40 min (3 x half-life) anticipated residence in the blood (20, 22, 23). Thus, the stronger effect of IV Gap27 is likely the result of its extra inhibitory effect on Cx37 hemichannels as indicated by earlier work (22). The contribution of Cx37 is further suggested from the poor protection of Cx43:Tie2-Cre^{POS} mice against barrier leakage, in which endothelial Cx37 expression was found to almost double, thereby obscuring Cx43-linked protection. This kind of compensatory alterations of vascular connexins upon knockout have been reported by others previously (88-91). In contrast to this, we found Cx37 to be lowered by LPS treatment although this did not attain statistical significance (**Fig. S1**). A question that remains is why Tat-Gap19 had more pronounced effects on barrier leakage when applied to the cortex compared to its systemic application (compare **Fig. 4A** with **Fig. 9C**). Possibly, Tat-Gap19 may have better bioavailability following direct loading into astrocytes as compared to its systemic injection.

Intravenous Tat-Gap19 and IV BAPTA-AM inhibited barrier leakage as well as GFAP elevation while IV Gap27 inhibited barrier leakage without tempering GFAP (non-significant effects, **Fig. 7B**), indicating that astrogliosis is not necessarily a direct consequence of barrier leakage *per se* in the LPS model. Rather, endothelial cells, activated by LPS or circulating cytokines, communicate with astrocytes by secreting immune factors that may induce astrogliosis (66, 67). Remarkably, neither IV BAPTA-AM nor IV Gap27 inhibited S100β appearance in the blood (non-significant effects, **Fig. 7D**) while IV Tat-Gap19 did. The absence of IV Gap27 effects is in line with the GFAP observations and results from poor penetration into the brain parenchyma. It is unclear why IV BAPTA-AM had no effect, as S100β, like GFAP (71-73), is activated by astrocytic

$[Ca^{2+}]_i$ elevation (44) and BAPTA-AM is expected to reduce S100β production as well as its passage through the BBB because of its endothelial effects preventing barrier leakage (**Fig. 4B**). Presumably, S100β activation may involve Ca^{2+}-independent effects.

To summarize, our data indicate that Cx43 in BBB endothelial cells and astrocytes plays a crucial role in barrier leakage induced by systemic inflammation that is mediated by the opening of hemichannels. In the blood, LPS as well as several pro-inflammatory cytokines trigger endothelial hemichannel opening while in the brain, IL6 activates astrocytic hemichannels. Cytoplasmic Ca^{2+} dynamics in these cells is intimately involved in triggering barrier leakage as a cause but also consequence of hemichannel opening. Targeting this connexin-Ca^{2+} axis in both brain endothelial cells and astrocytes is therefore an effective approach, resulting in suppression of barrier leakage as well as astrogliosis. Extending the spectrum of hemichannel inhibitor substances to vascular connexins other than Cx43 may further improve the efficiency of preventing inflammatory barrier leakage.

Methods

A detailed description of all procedures can be found in the supplemental data file.

Animals

Mice were treated according to the European Ethics Committee guidelines and the study protocol was approved by the animal experiment ethical committee of the Faculty (Medicine and Health Sciences, Ghent University). Experiments were performed in male FVB mice, inducible global Cx43Cre-ER(T)/fl mice (kindly provided by Dr. R. Schulz, Justus-Liebig University, Giessen, Germany), global Cx30 KO and Cx30KO/Cx43fl:GFAP-Cre "double KO" mice and Cx43fl:Tie2Cre endothelial Cx43 KO (kindly provided by Dr. D. Krysko, Ghent University).

Adult mice (25-30g, aged 6-12 weeks) received an intraperitoneal (IP) bolus injection of LPS (freshly dissolved in filter-sterilized saline (0.9 % NaCl) prior to injection). Mice received a single

intravenous (IV) bolus injection of Gap27 (25 mg/kg; 200 µM in blood volume) or Tat-Gap19 (54 mg/kg; 200 µM in blood volume) freshly dissolved in filter-sterilized saline, immediately before IP LPS injection. Control peptides were administered in an identical manner. Vehicle control mice received an IV injection with saline only, prior to LPS. The half-life of Gap27 and Tat-Gap19 peptides was calculated with the peptide lifetime predictor (PlifePred, http://crdd.osdd.net/raghava/plifepred/) as described in (34). BAPTA-AM was prepared at a concentration of 33 mM in DMSO and 0.16 % pluronic acid, and further diluted in sterile saline to a final concentration of 2 mM or 12 mg/kg (+ 0.01% pluronic acid). BAPTA-AM was administered IV, 30 min prior to IP LPS injection. Vehicle control mice received a bolus injection of DMSO + pluronic acid dissolved in sterile saline.

Blood-brain barrier permeability

Ten minutes prior to decapitation, mice received an intravenous (IV) bolus (200 µL) of 3 kDa dextran fluorescein (DF; 30 mg/kg), 10 kDa dextran texas red (DTR; 100 mg/kg), or FITC-albumin (66 kDa; 660 mg/kg), through tail vein injection, each dye ultimately reaching an estimated 200 µM in the blood compartment. Subsequently, animals were transcardially perfused, brains were isolated and snap-frozen. Parenchymal fluorescence was quantified in coronal brain cryosections and expressed relative to the signal observed in non-treated control animals (number of animals as in the treated group).

Cranial window

A craniotomy was made in the right parietal bone covering the somatosensorial cortex (details see Supplemental data) and artificial cerebrospinal fluid containing sulforhodamine 101 (SR101, 50 µM) to mark astrocytes was applied to the exposed cortex. For interventions targeting $[Ca^{2+}]_i$ or Cx43 hemichannels, BAPTA-AM (2 mM) or Tat-Gap19 (200 µM) were included in the solution. Subsequently, LPS was injected IP and animals were allowed to recover. At 3, 6 and 24 h mice were anesthetized for barrier permeability measurements as described above. Cortical fluorescence intensity was measured in the SR101 loaded region.

For cortical hemichannel dye uptake experiments, ethidium bromide (EtBr, 100 µM) was added to the exposed cortex 30 min before sacrifice. Thereafter, mice were transcardially perfused. EtBr positive cells were counted in coronal brain sections and expressed relative to the number of nuclei.

Electrophysiological Recording

See supplementary material

Calcium imaging

Cells were loaded with the Ca^{2+} indicator dye fluo3-AM and transferred to an inverted epifluorescence microscope (Eclipse TE 300, Nikon Belux), equipped with a superfusion system that allowed fast solution switching. Ca^{2+} oscillations were counted in a 10 min observation period and were defined as at least two transient Ca^{2+} changes after the initial Ca^{2+} transient in a single cell, minimally 5 % above baseline fluo3-fluorescence.

Immunohistochemistry

Immunohistochemical analysis of protein expression was performed on coronal mouse brain cryosections or freshly isolated capillaries (see Cell isolation and cell culture studies in Supplemental data), excluding enzymatic digestion and subsequent steps). Primary antibodies were rat anti-CD31 (Invitrogen/BD Biosciences), rabbit anti-AQP4 (Merck Millipore), rabbit-GFAP (Abcam), GFAP-Cy3 (Invitrogen), rabbit anti-Cx43 (Sigma-Aldrich) and mouse anti-Cx43 (Merck Millipore/BD Biosciences). Further details on antibodies used can be found in the Supplemental data file.

Gel electrophoresis and western blotting

Cell lysates and plasma samples were separated by electrophoresis over a 4-12 % SDS-polyacrylamide gel and transferred to a nitrocellulose membrane. Blots were probed with rabbit anti-Cx43 antibody (Sigma-Aldrich) or rabbit anti-S100β (Abcam, Cambridge, UK). Quantification was done using ImageJ. Other antibodies used in western blotting experiments presented as Supplemental data are specified there.

Statistics

Data are expressed as mean ± S.E.M. with n giving the number of independent experiments (indicated on the corresponding bar) and statistical analysis was performed using Graphpad software. Occasional outliers were removed making use of GraphPad QuickCalcs Outlier calculator. Normality of the distributions was verified with the Kolmogorov-Smirnov test; all data were normally distributed except for the IL1β and TNFα data that deviated from normality. Data expressed relative to data obtained in an associated non-treated control group (Fig. 1C, Fig. 2A, Fig. 3, Fig. 7B and D, Fig. 8) were compared to the control 100 % level by a one-sample t-test. Two groups were compared with a two-sample Student's t-test. Multiple groups were compared by one-way ANOVA with Bonferroni post-hoc testing; Dunnett testing was used for repeated comparisons to a defined control condition. Time series data were compared by repeated measures ANOVA with Dunnett's post-hoc test. Non-parametric Kruskal-Wallis testing was done for IL1β and TNFα data (Fig. 1D and Fig. S1A in Supplemental data). Results were considered statistically significant when $p<0.05$ (one symbol for $p<0.05$, two for $p<0.01$ and three for $p<0.001$).

Author Contributions

M.D.B, M.D.S, S.V. H.T., S.S. and V.V.H. designed and conducted experiments; , K.W., C.S., N.R. and R.E.V. provided experimental and analytical tools and expertise; M.D.B and L.L. wrote the manuscript with input from all authors; M.D.B and L.L. supervised the project. Co-first authorship was decided based on leadership (M.D.B) and crucial contributions to functional hemichannel assessment and experiments (M.D.S.).

Acknowledgements

We are very grateful for the proficient help and technical assistance of Ellen Cocquyt, Thi Thu Hang Dang and Diego De Baere (Dept. Basic and Applied Medical Sciences), and Elien Van Wontergem and Griet Van Imschoot (Inflammation Research Center, Flemish Institute of Biotechnology). We appreciate the expertise and advice of Em. Prof. Dr. Gaspard De Ley for cranial window preparation.

This work was supported by the Fund for Scientific Research Flanders, Belgium (grant nos. G.0A82.13N, G.0320.15N and G052718N to L.L.) and the Geneeskundige Stichting Koningin Elisabeth (grant STI.DI2.2017.0004.01 to L.L.). Maarten De Smet was supported by a personal grant from the Fund for Scientific Research Flanders (1124418N).

References

1. Liebner S, Dijkhuizen RM, Reiss Y, Plate KH, Agalliu D, and Constantin G. Functional morphology of the blood-brain barrier in health and disease. *Acta neuropathologica.* 2018;135(3):311-36.
2. Alvarez JI, Katayama T, and Prat A. Glial influence on the blood brain barrier. *Glia.* 2013;61(12):1939-58.
3. Abbott NJ, Ronnback L, and Hansson E. Astrocyte-endothelial interactions at the blood-brain barrier. *Nature reviews Neuroscience.* 2006;7(1):41-53.
4. Cheslow L, and Alvarez JI. Glial-endothelial crosstalk regulates blood-brain barrier function. *Current opinion in pharmacology.* 2016;26:39-46.
5. De Bock M, Leybaert L, and Giaume C. Connexin Channels at the Glio-Vascular Interface: Gatekeepers of the Brain. *Neurochemical research.* 2017;42(9):2519-36.
6. Ezan P, Andre P, Cisternino S, Saubamea B, Boulay AC, Doutremer S, et al. Deletion of astroglial connexins weakens the blood-brain barrier. *Journal of cerebral blood flow and metabolism : official journal of the International Society of Cerebral Blood Flow and Metabolism.* 2012;32(8):1457-67.
7. Simard M, Arcuino G, Takano T, Liu QS, and Nedergaard M. Signaling at the gliovascular interface. *The Journal of neuroscience : the official journal of the Society for Neuroscience.* 2003;23(27):9254-62.
8. Xu HL, Mao L, Ye S, Paisansathan C, Vetri F, and Pelligrino DA. Astrocytes are a key conduit for upstream signaling of vasodilation during cerebral cortical neuronal activation in vivo. *Am J Physiol Heart Circ Physiol.* 2008;294(2):H622-32.
9. Otsu Y, Couchman K, Lyons DG, Collot M, Agarwal A, Mallet JM, et al. Calcium dynamics in astrocyte processes during neurovascular coupling. *Nature neuroscience.* 2015;18(2):210-8.
10. Mulligan SJ, and MacVicar BA. Calcium transients in astrocyte endfeet cause cerebrovascular constrictions. *Nature.* 2004;431(7005):195-9.
11. Boulay AC, Mazeraud A, Cisternino S, Saubamea B, Mailly P, Jourdren L, et al. Immune quiescence of the brain is set by astroglial connexin 43. *The Journal of neuroscience : the official journal of the Society for Neuroscience.* 2015;35(10):4427-39.
12. Mallard C. Innate immune regulation by toll-like receptors in the brain. *ISRN Neurol.* 2012;2012:701950.
13. Tarassishin L, Suh HS, and Lee SC. LPS and IL-1 differentially activate mouse and human astrocytes: role of CD14. *Glia.* 2014;62(6):999-1013.
14. Wilhelm I, Nyul-Toth A, Kozma M, Farkas AE, and Krizbai IA. Role of pattern recognition receptors of the neurovascular unit in inflamm-aging. *Am J Physiol Heart Circ Physiol.* 2017;313(5):H1000-H12.
15. Biesmans S, Matthews LJ, Bouwknecht JA, De Haes P, Hellings N, Meert TF, et al. Systematic Analysis of the Cytokine and Anhedonia Response to Peripheral Lipopolysaccharide Administration in Rats. *Biomed Res Int.* 2016;2016:9085273.
16. Biesmans S, Meert TF, Bouwknecht JA, Acton PD, Davoodi N, De Haes P, et al. Systemic immune activation leads to neuroinflammation and sickness behavior in mice. *Mediators of inflammation.* 2013;2013:271359.
17. Cronin M, Anderson PN, Cook JE, Green CR, and Becker DL. Blocking connexin43 expression reduces inflammation and improves functional recovery after spinal cord injury. *Molecular and cellular neurosciences.* 2008;39(2):152-60.
18. Danesh-Meyer HV, Kerr NM, Zhang J, Eady EK, O'Carroll SJ, Nicholson LF, et al. Connexin43 mimetic peptide reduces vascular leak and retinal ganglion cell death following retinal ischaemia. *Brain : a journal of neurology.* 2012;135(Pt 2):506-20.

19. Johnson AM, Roach JP, Hu A, Stamatovic SM, Zochowski MR, Keep RF, et al. Connexin 43 gap junctions contribute to brain endothelial barrier hyperpermeability in familial cerebral cavernous malformations type III by modulating tight junction structure. *FASEB journal : official publication of the Federation of American Societies for Experimental Biology.* 2018:fj201700699R.
20. Decrock E, De Vuyst E, Vinken M, Van Moorhem M, Vranckx K, Wang N, et al. Connexin 43 hemichannels contribute to the propagation of apoptotic cell death in a rat C6 glioma cell model. *Cell death and differentiation.* 2009;16(1):151-63.
21. Desplantez T, Verma V, Leybaert L, Evans WH, and Weingart R. Gap26, a connexin mimetic peptide, inhibits currents carried by connexin43 hemichannels and gap junction channels. *Pharmacological research.* 2012;65(5):546-52.
22. De Bock M, Culot M, Wang N, Bol M, Decrock E, De Vuyst E, et al. Connexin channels provide a target to manipulate brain endothelial calcium dynamics and blood-brain barrier permeability. *Journal of cerebral blood flow and metabolism : official journal of the International Society of Cerebral Blood Flow and Metabolism.* 2011;31(9):1942-57.
23. Wang N, De Bock M, Antoons G, Gadicherla AK, Bol M, Decrock E, et al. Connexin mimetic peptides inhibit Cx43 hemichannel opening triggered by voltage and intracellular Ca2+ elevation. *Basic research in cardiology.* 2012;107(6):304.
24. Leybaert L, Lampe PD, Dhein S, Kwak BR, Ferdinandy P, Beyer EC, et al. Connexins in Cardiovascular and Neurovascular Health and Disease: Pharmacological Implications. *Pharmacol Rev.* 2017;69(4):396-478.
25. Abudara V, Bechberger J, Freitas-Andrade M, De Bock M, Wang N, Bultynck G, et al. The connexin43 mimetic peptide Gap19 inhibits hemichannels without altering gap junctional communication in astrocytes. *Frontiers in cellular neuroscience.* 2014;8:306.
26. Freitas-Andrade M, Wang N, Bechberger JF, De Bock M, Lampe PD, Leybaert L, et al. Targeting MAPK phosphorylation of Connexin43 provides neuroprotection in stroke. *The Journal of experimental medicine.* 2019;216(4):916-35.
27. De Bock M, Culot M, Wang N, da Costa A, Decrock E, Bol M, et al. Low extracellular Ca2+ conditions induce an increase in brain endothelial permeability that involves intercellular Ca2+ waves. *Brain research.* 2012;1487:78-87.
28. Tymianski M, Spigelman I, Zhang L, Carlen PL, Tator CH, Charlton MP, et al. Mechanism of action and persistence of neuroprotection by cell-permeant Ca2+ chelators. *Journal of cerebral blood flow and metabolism : official journal of the International Society of Cerebral Blood Flow and Metabolism.* 1994;14(6):911-23.
29. Tonkikh A, Janus C, El-Beheiry H, Pennefather PS, Samoilova M, McDonald P, et al. Calcium chelation improves spatial learning and synaptic plasticity in aged rats. *Exp Neurol.* 2006;197(2):291-300.
30. Lutz SE, Zhao Y, Gulinello M, Lee SC, Raine CS, and Brosnan CF. Deletion of astrocyte connexins 43 and 30 leads to a dysmyelinating phenotype and hippocampal CA1 vacuolation. *The Journal of neuroscience : the official journal of the Society for Neuroscience.* 2009;29(24):7743-52.
31. Wallraff A, Kohling R, Heinemann U, Theis M, Willecke K, and Steinhauser C. The impact of astrocytic gap junctional coupling on potassium buffering in the hippocampus. *The Journal of neuroscience : the official journal of the Society for Neuroscience.* 2006;26(20):5438-47.
32. Lutz SE, Raine CS, and Brosnan CF. Loss of astrocyte connexins 43 and 30 does not significantly alter susceptibility or severity of acute experimental autoimmune encephalomyelitis in mice. *Journal of neuroimmunology.* 2012;245(1-2):8-14.
33. Cibelli A, Stout R, Timmermann A, de Menezes L, Guo P, Maass K, et al. Cx43 carboxyl terminal domain determines AQP4 and Cx30 endfoot organization and blood brain barrier permeability. *Scientific reports.* 2021;11(1):24334.

34. Mathur D, Singh S, Mehta A, Agrawal P, and Raghava GPS. In silico approaches for predicting the half-life of natural and modified peptides in blood. *PloS one.* 2018;13(6):e0196829.
35. Retamal MA, Froger N, Palacios-Prado N, Ezan P, Saez PJ, Saez JC, et al. Cx43 hemichannels and gap junction channels in astrocytes are regulated oppositely by proinflammatory cytokines released from activated microglia. *The Journal of neuroscience : the official journal of the Society for Neuroscience.* 2007;27(50):13781-92.
36. Saez JC, Contreras-Duarte S, Gomez GI, Labra VC, Santibanez CA, Gajardo-Gomez R, et al. Connexin 43 Hemichannel Activity Promoted by Pro-Inflammatory Cytokines and High Glucose Alters Endothelial Cell Function. *Front Immunol.* 2018;9:1899.
37. Anderson MA, Ao Y, and Sofroniew MV. Heterogeneity of reactive astrocytes. *Neuroscience letters.* 2014;565:23-9.
38. Donato R, Sorci G, Riuzzi F, Arcuri C, Bianchi R, Brozzi F, et al. S100B's double life: intracellular regulator and extracellular signal. *Biochimica et biophysica acta.* 2009;1793(6):1008-22.
39. Kanner AA, Marchi N, Fazio V, Mayberg MR, Koltz MT, Siomin V, et al. Serum S100beta: a noninvasive marker of blood-brain barrier function and brain lesions. *Cancer.* 2003;97(11):2806-13.
40. Michetti F, D'Ambrosi N, Toesca A, Puglisi MA, Serrano A, Marchese E, et al. The S100B story: from biomarker to active factor in neural injury. *Journal of neurochemistry.* 2018.
41. Guerra MC, Tortorelli LS, Galland F, Da Re C, Negri E, Engelke DS, et al. Lipopolysaccharide modulates astrocytic S100B secretion: a study in cerebrospinal fluid and astrocyte cultures from rats. *Journal of neuroinflammation.* 2011;8:128.
42. Edwards MM, and Robinson SR. TNF alpha affects the expression of GFAP and S100B: implications for Alzheimer's disease. *Journal of neural transmission.* 2006;113(11):1709-15.
43. Sheng JG, Ito K, Skinner RD, Mrak RE, Rovnaghi CR, Van Eldik LJ, et al. In vivo and in vitro evidence supporting a role for the inflammatory cytokine interleukin-1 as a driving force in Alzheimer pathogenesis. *Neurobiology of aging.* 1996;17(5):761-6.
44. Davey GE, Murmann P, and Heizmann CW. Intracellular Ca2+ and Zn2+ levels regulate the alternative cell density-dependent secretion of S100B in human glioblastoma cells. *The Journal of biological chemistry.* 2001;276(33):30819-26.
45. Nimmerjahn A, Kirchhoff F, Kerr JN, and Helmchen F. Sulforhodamine 101 as a specific marker of astroglia in the neocortex in vivo. *Nat Methods.* 2004;1(1):31-7.
46. Schnell C, Shahmoradi A, Wichert SP, Mayerl S, Hagos Y, Heuer H, et al. The multispecific thyroid hormone transporter OATP1C1 mediates cell-specific sulforhodamine 101-labeling of hippocampal astrocytes. *Brain Struct Funct.* 2015;220(1):193-203.
47. Ding S. In vivo imaging of Ca(2)(+) signaling in astrocytes using two-photon laser scanning fluorescent microscopy. *Methods in molecular biology.* 2012;814:545-54.
48. Hirase H, Qian L, Bartho P, and Buzsaki G. Calcium dynamics of cortical astrocytic networks in vivo. *PLoS biology.* 2004;2(4):E96.
49. Tian GF, Takano T, Lin JH, Wang X, Bekar L, and Nedergaard M. Imaging of cortical astrocytes using 2-photon laser scanning microscopy in the intact mouse brain. *Adv Drug Deliv Rev.* 2006;58(7):773-87.
50. Froger N, Orellana JA, Calvo CF, Amigou E, Kozoriz MG, Naus CC, et al. Inhibition of cytokine-induced connexin43 hemichannel activity in astrocytes is neuroprotective. *Molecular and cellular neurosciences.* 2010;45(1):37-46.
51. Abudara V, Roux L, Dallerac G, Matias I, Dulong J, Mothet JP, et al. Activated microglia impairs neuroglial interaction by opening Cx43 hemichannels in hippocampal astrocytes. *Glia.* 2015;63(5):795-811.

52. Meunier C, Wang N, Yi C, Dallerac G, Ezan P, Koulakoff A, et al. Contribution of Astroglial Cx43 Hemichannels to the Modulation of Glutamatergic Currents by D-Serine in the Mouse Prefrontal Cortex. *The Journal of neuroscience : the official journal of the Society for Neuroscience.* 2017;37(37):9064-75.
53. Banks WA, and Robinson SM. Minimal penetration of lipopolysaccharide across the murine blood-brain barrier. *Brain, behavior, and immunity.* 2010;24(1):102-9.
54. Singh AK, and Jiang Y. How does peripheral lipopolysaccharide induce gene expression in the brain of rats? *Toxicology.* 2004;201(1-3):197-207.
55. Miller SI, Ernst RK, and Bader MW. LPS, TLR4 and infectious disease diversity. *Nat Rev Microbiol.* 2005;3(1):36-46.
56. Saijo K, and Glass CK. Microglial cell origin and phenotypes in health and disease. *Nature reviews Immunology.* 2011;11(11):775-87.
57. de Vries HE, Blom-Roosemalen MC, van Oosten M, de Boer AG, van Berkel TJ, Breimer DD, et al. The influence of cytokines on the integrity of the blood-brain barrier in vitro. *Journal of neuroimmunology.* 1996;64(1):37-43.
58. Deli MA, Descamps L, Dehouck MP, Cecchelli R, Joo F, Abraham CS, et al. Exposure of tumor necrosis factor-alpha to luminal membrane of bovine brain capillary endothelial cells cocultured with astrocytes induces a delayed increase of permeability and cytoplasmic stress fiber formation of actin. *Journal of neuroscience research.* 1995;41(6):717-26.
59. Raasch M, Rennert K, Jahn T, Gartner C, Schonfelder G, Huber O, et al. An integrative microfluidically supported in vitro model of an endothelial barrier combined with cortical spheroids simulates effects of neuroinflammation in neocortex development. *Biomicrofluidics.* 2016;10(4):044102.
60. De Bock M, Wang N, Decrock E, Bol M, Gadicherla AK, Culot M, et al. Endothelial calcium dynamics, connexin channels and blood-brain barrier function. *Progress in neurobiology.* 2013;108:1-20.
61. Campbell IL, Erta M, Lim SL, Frausto R, May U, Rose-John S, et al. Trans-signaling is a dominant mechanism for the pathogenic actions of interleukin-6 in the brain. *The Journal of neuroscience : the official journal of the Society for Neuroscience.* 2014;34(7):2503-13.
62. von Banchet GS, Kiehl M, and Schaible HG. Acute and long-term effects of IL-6 on cultured dorsal root ganglion neurones from adult rat. *Journal of neurochemistry.* 2005;94(1):238-48.
63. Erta M, Quintana A, and Hidalgo J. Interleukin-6, a major cytokine in the central nervous system. *Int J Biol Sci.* 2012;8(9):1254-66.
64. Vallieres L, and Rivest S. Regulation of the genes encoding interleukin-6, its receptor, and gp130 in the rat brain in response to the immune activator lipopolysaccharide and the proinflammatory cytokine interleukin-1beta. *Journal of neurochemistry.* 1997;69(4):1668-83.
65. Hasegawa-Ishii S, Inaba M, Umegaki H, Unno K, Wakabayashi K, and Shimada A. Endotoxemia-induced cytokine-mediated responses of hippocampal astrocytes transmitted by cells of the brain-immune interface. *Scientific reports.* 2016;6:25457.
66. Grab DJ, Chakravorty SJ, van der Heyde H, and Stins MF. How can microbial interactions with the blood-brain barrier modulate astroglial and neuronal function? *Cell Microbiol.* 2011;13(10):1470-8.
67. Varatharaj A, and Galea I. The blood-brain barrier in systemic inflammation. *Brain, behavior, and immunity.* 2016.
68. De Bock M, Wang N, Bol M, Decrock E, Ponsaerts R, Bultynck G, et al. Connexin 43 hemichannels contribute to cytoplasmic Ca2+ oscillations by providing a bimodal Ca2+-dependent Ca2+ entry pathway. *The Journal of biological chemistry.* 2012;287(15):12250-66.

69. Sofroniew MV. Astrocyte barriers to neurotoxic inflammation. *Nature reviews Neuroscience.* 2015;16(5):249-63.
70. Zamanian JL, Xu L, Foo LC, Nouri N, Zhou L, Giffard RG, et al. Genomic analysis of reactive astrogliosis. *The Journal of neuroscience : the official journal of the Society for Neuroscience.* 2012;32(18):6391-410.
71. Gao K, Wang CR, Jiang F, Wong AY, Su N, Jiang JH, et al. Traumatic scratch injury in astrocytes triggers calcium influx to activate the JNK/c-Jun/AP-1 pathway and switch on GFAP expression. *Glia.* 2013;61(12):2063-77.
72. Lee YB, Du S, Rhim H, Lee EB, Markelonis GJ, and Oh TH. Rapid increase in immunoreactivity to GFAP in astrocytes in vitro induced by acidic pH is mediated by calcium influx and calpain I. *Brain research.* 2000;864(2):220-9.
73. Salazar M, Pariente JA, Salido GM, and Gonzalez A. Ebselen increases cytosolic free Ca2+ concentration, stimulates glutamate release and increases GFAP content in rat hippocampal astrocytes. *Toxicology.* 2008;244(2-3):280-91.
74. Biesecker KR, Srienc AI, Shimoda AM, Agarwal A, Bergles DE, Kofuji P, et al. Glial Cell Calcium Signaling Mediates Capillary Regulation of Blood Flow in the Retina. *The Journal of neuroscience : the official journal of the Society for Neuroscience.* 2016;36(36):9435-45.
75. Mishra A, Reynolds JP, Chen Y, Gourine AV, Rusakov DA, and Attwell D. Astrocytes mediate neurovascular signaling to capillary pericytes but not to arterioles. *Nature neuroscience.* 2016;19(12):1619-27.
76. Iadecola C. The Neurovascular Unit Coming of Age: A Journey through Neurovascular Coupling in Health and Disease. *Neuron.* 2017;96(1):17-42.
77. Bynoe MS, Viret C, Yan A, and Kim DG. Adenosine receptor signaling: a key to opening the blood-brain door. *Fluids and barriers of the CNS.* 2015;12:20.
78. Carman AJ, Mills JH, Krenz A, Kim DG, and Bynoe MS. Adenosine receptor signaling modulates permeability of the blood-brain barrier. *The Journal of neuroscience : the official journal of the Society for Neuroscience.* 2011;31(37):13272-80.
79. Frankowski JC, DeMars KM, Ahmad AS, Hawkins KE, Yang C, Leclerc JL, et al. Detrimental role of the EP1 prostanoid receptor in blood-brain barrier damage following experimental ischemic stroke. *Scientific reports.* 2015;5:17956.
80. Hurtado-Alvarado G, Dominguez-Salazar E, Velazquez-Moctezuma J, and Gomez-Gonzalez B. A2A Adenosine Receptor Antagonism Reverts the Blood-Brain Barrier Dysfunction Induced by Sleep Restriction. *PloS one.* 2016;11(11):e0167236.
81. Kim DG, and Bynoe MS. A2A Adenosine Receptor Regulates the Human Blood-Brain Barrier Permeability. *Molecular neurobiology.* 2015;52(1):664-78.
82. Leclerc JL, Lampert AS, Diller MA, Immergluck JB, and Dore S. Prostaglandin E2 EP2 receptor deletion attenuates intracerebral hemorrhage-induced brain injury and improves functional recovery. *ASN neuro.* 2015;7(2).
83. Bartnik BL, Spigelman I, and Obenaus A. Cell-permeant calcium buffer induced neuroprotection after cortical devascularization. *Exp Neurol.* 2005;192(2):357-64.
84. Ikegaya Y, Le Bon-Jego M, and Yuste R. Large-scale imaging of cortical network activity with calcium indicators. *Neurosci Res.* 2005;52(2):132-8.
85. Wang N, De Vuyst E, Ponsaerts R, Boengler K, Palacios-Prado N, Wauman J, et al. Selective inhibition of Cx43 hemichannels by Gap19 and its impact on myocardial ischemia/reperfusion injury. *Basic research in cardiology.* 2013;108(1):309.
86. Walrave L, Vinken M, Albertini G, De Bundel D, Leybaert L, and Smolders IJ. Inhibition of Connexin43 Hemichannels Impairs Spatial Short-Term Memory without Affecting Spatial Working Memory. *Frontiers in cellular neuroscience.* 2016;10:288.

87. Maatouk L, Yi C, Carrillo-de Sauvage MA, Compagnion AC, Hunot S, Ezan P, et al. Glucocorticoid receptor in astrocytes regulates midbrain dopamine neurodegeneration through connexin hemichannel activity. *Cell death and differentiation.* 2018.
88. Bedner P, Steinhauser C, and Theis M. Functional redundancy and compensation among members of gap junction protein families? *Biochimica et biophysica acta.* 2012;1818(8):1971-84.
89. Figueroa XF, and Duling BR. Gap junctions in the control of vascular function. *Antioxidants & redox signaling.* 2009;11(2):251-66.
90. Simon AM, and McWhorter AR. Decreased intercellular dye-transfer and downregulation of non-ablated connexins in aortic endothelium deficient in connexin37 or connexin40. *Journal of cell science.* 2003;116(Pt 11):2223-36.
91. Simon AM, McWhorter AR, Dones JA, Jackson CL, and Chen H. Heart and head defects in mice lacking pairs of connexins. *Dev Biol.* 2004;265(2):369-83.

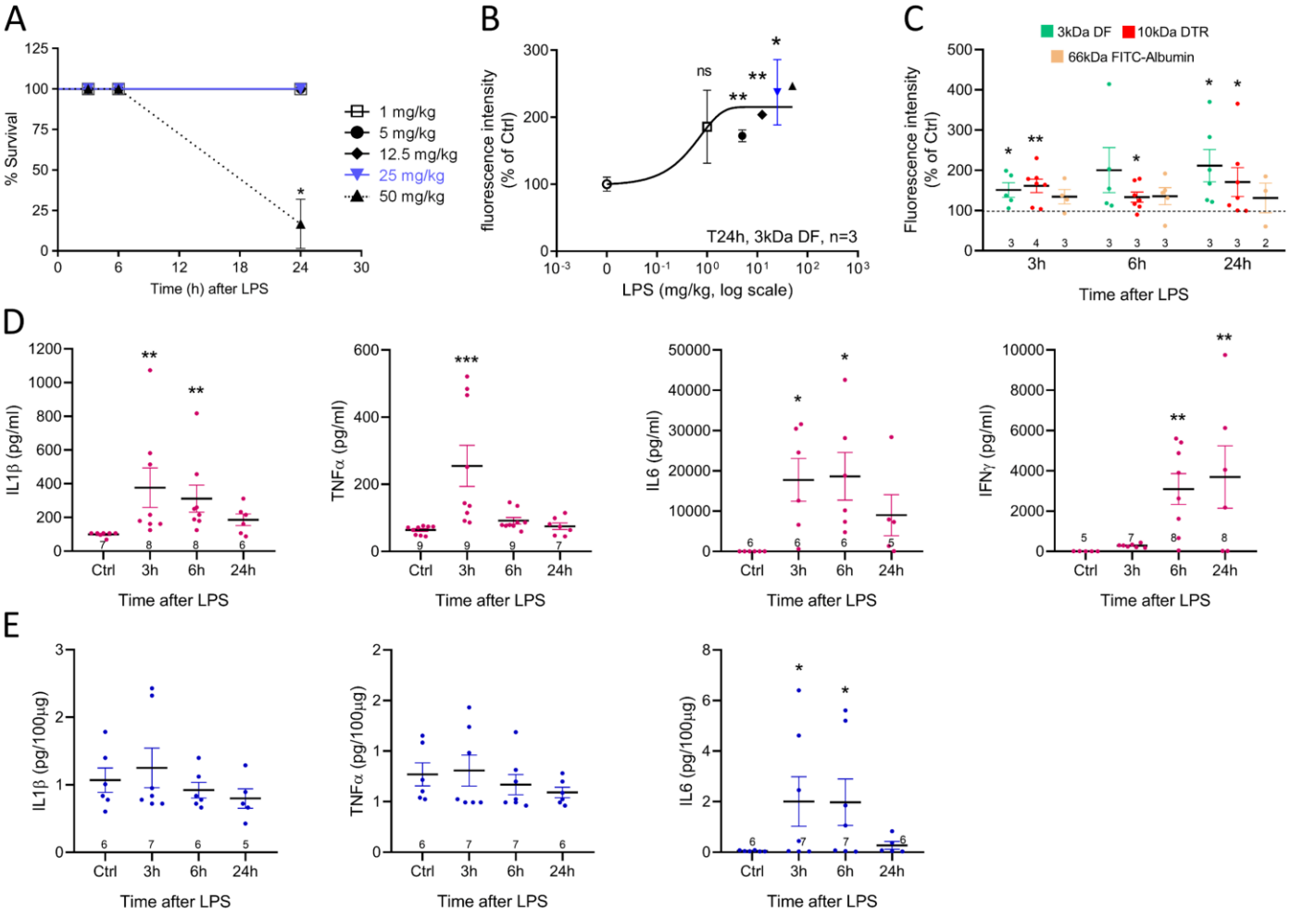

Figure 1. LPS-induced BBB leakage and inflammation in mice. A. Kaplan-Meier plot illustrating survival for increasing doses of IP-injected LPS. With exception of the highest dose (50 mg/kg), LPS did not affect survival (n = 3 for 1-5-12.5 and 25mg/kg and n = 6 for 50 mg/kg; for the 1-25 mg/kg dose range, survival is 100 % and data points therefore overlap). **B.** Dose-response curve for BBB leakage of 3kDa dextran fluorescein (DF) (IV 30 mg/kg), 24 h post-LPS. Leakage increased with increasing LPS dose, reaching a plateau at 25-50 mg/kg. (Mean ± S.E.M. with n = 3 for all concentrations, except for 50 mg/kg where n = 1 due to high mortality; Dunnett test comparison to no LPS). Symbols correspond to panel A. The 25 mg/kg dose was used in all further experiments (marked in blue). **C.** LPS-induced BBB leakage at 3, 6 and 24 h post-LPS, determined with 3 kDa DF (30 mg/kg), 10 kDa dextran Texas red (DTR; 100 mg/kg), and FITC-Albumin (66 kDa, 660 mg/kg). Stars compare to Ctrl (saline IP; one-sample t-test). Numbers in the bars indicate experiments on different animals. **D-E.** Plasma and brain levels of IL1β, TNFα, IFNγ and IL6 following LPS. In plasma (D), all tested cytokines were significantly elevated; IFNγ showed a delayed response. In the brain (E), only IL6 increased with a time course as in plasma; IL1β and TNFα were not increased, and IFNγ was not detectable. Stars indicate significant difference with Ctrl (saline IP; one-way ANOVA, Dunnett test except for IL1β & TNFα where non-parametric Kruskal-Wallis testing was used).

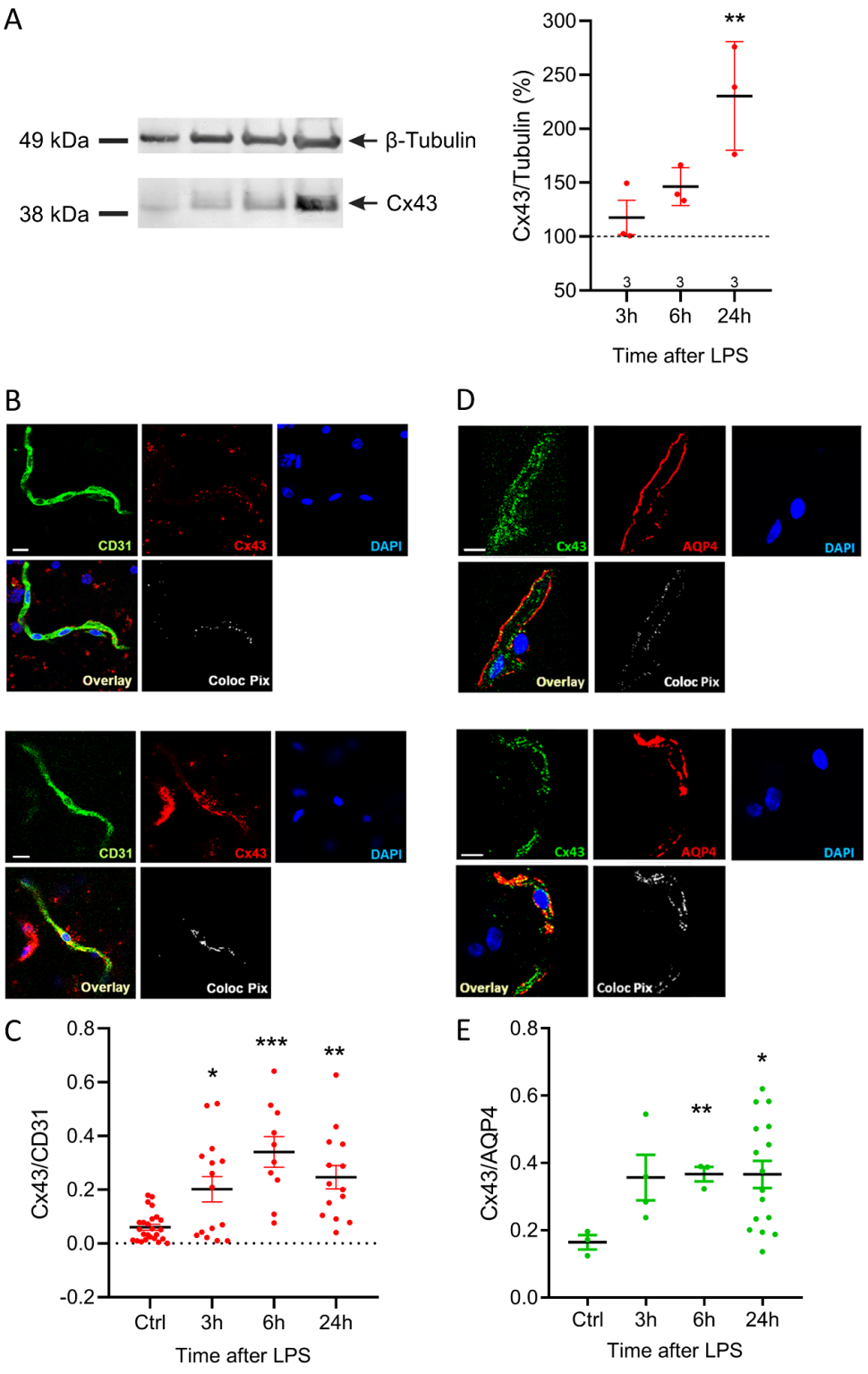

Figure 2. Cx43 expression increases after IP LPS treatment. A. SDS-PAGE and Western blotting experiments showed a strong Cx43 increase in freshly isolated mouse brain capillary endothelial cells treated with LPS (1 µg/mL) (one-sample t-test). **B.** Staining for the endothelial cell marker CD31 and Cx43 in isolated brain capillaries of Ctrl and LPS-injected mice (25 mg/kg). Pixels in white (Coloc Pix, size 180 nm^2) illustrate combined Cx43/CD31 positivity. Scale bar is 10 µm. **C.** Summary white Coloc pixel counts of experiments as in B, illustrating strongly increased Cx43 expression in brain capillary endothelial cells in animals that received LPS. **D-E.** Colocalization analysis of Cx43 and the astrocytic endfeet marker AQP4 demonstrated increased Cx43 expression in endfeet remnants in capillaries of animals that received LPS. Stars in C & E indicate significant difference compared to normalized Ctrl (one-way ANOVA, Dunnett test).

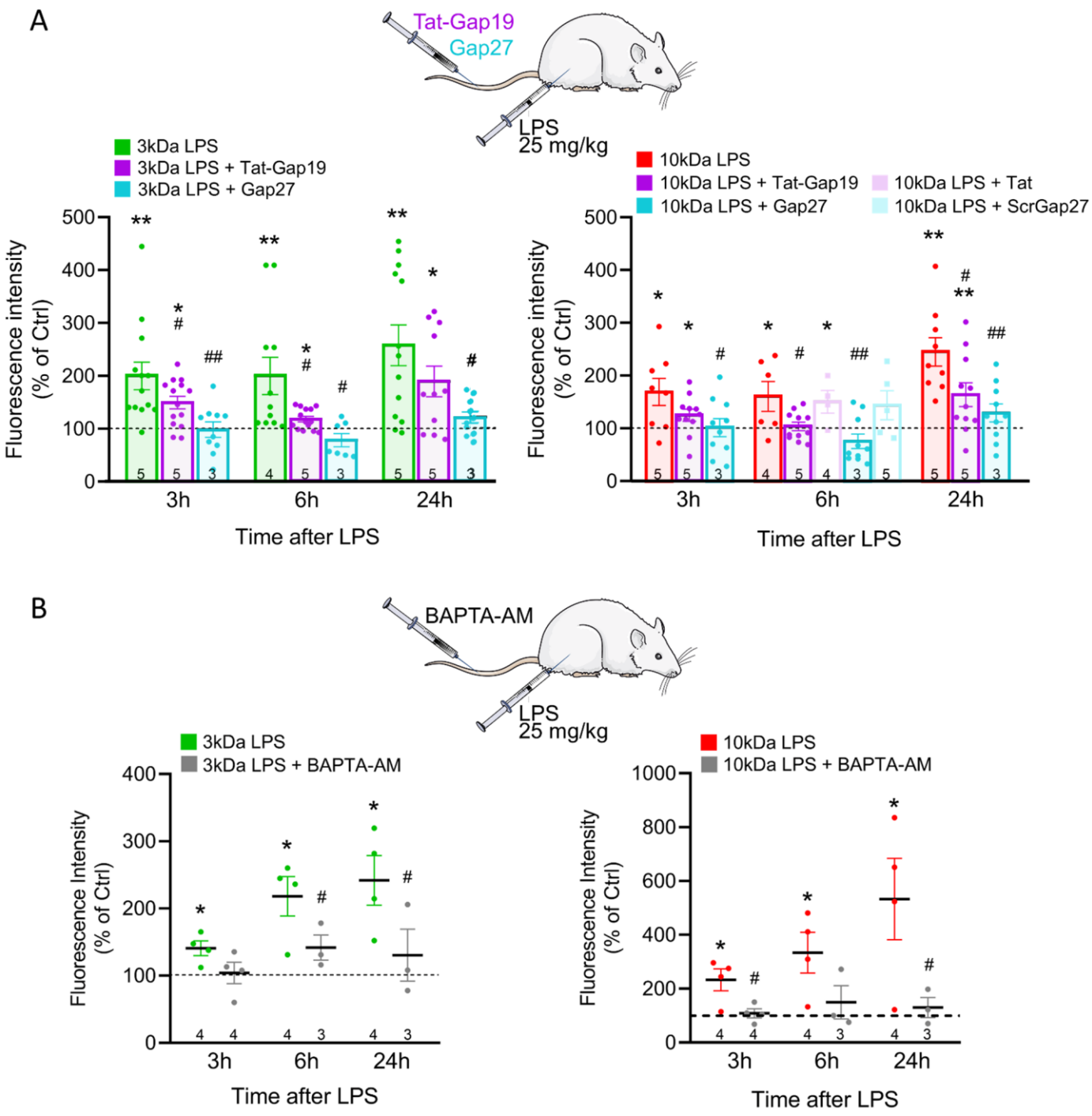

Figure 3. Gap27, Tat-Gap19 and intracellular Ca^{2+} chelation with BAPTA-AM reduce LPS-induced BBB leakage. A. IV injection of Gap27 (25 mg/kg) or Tat-Gap19 (54 mg/kg) immediately (< 1 min) before IP administration of LPS (25 mg/kg) prevented BBB leakage to 3 kDa DF and 10 kDa DTR. Scrambled Gap27 or Tat peptide not linked to Gap19, had no effect (open bars at 6 h 10 kDa). Stars indicate significant elevation above Ctrl (one-sample t-test); number signs indicate significant reduction compared to LPS-only (one-way ANOVA, Dunnett test). **B.** IV injection of the intracellular Ca^{2+} chelator BAPTA-AM, 30 min prior to LPS reduced the 3 and 10 kDa tracer leakage. Stars indicate significant elevation above Ctrl (one-sample t-test); number signs indicate significant reduction compared to LPS-only (two-sample t-test).

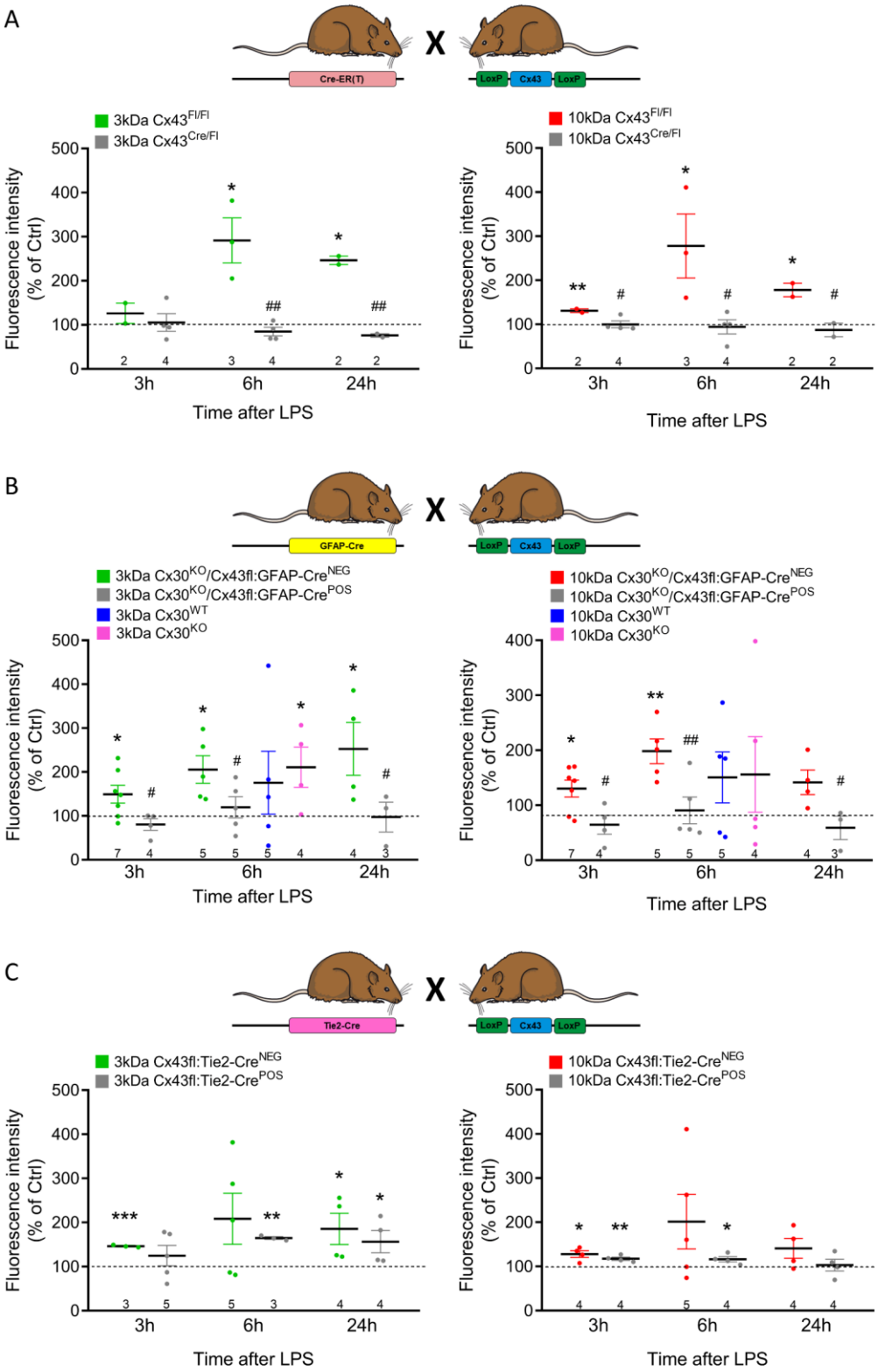

Figure 4. LPS-induced BBB leakage is reduced in various Cx43 knockout mice. A. Effect of global Cx43 knockdown. BBB leakage in tamoxifen-treated $Cx43^{Cre\text{-}ER(T)/Fl}$ mice was strongly reduced compared to tamoxifen treated $Cx43^{Fl/Fl}$ littermates that still fully express Cx43. **B.** Effect of astrocyte-specific Cx43 knockout combined with global Cx30 knockout (double KO) and of Cx30 knockout only. BBB leakage in $Cx30^{KO}$/Cx43fl:GFAP-Cre^{POS} mice was strongly reduced compared to $Cx30^{KO}$/Cx43fl:GFAP-Cre^{NEG} littermates. Open bars show BBB leakage in $Cx30^{KO}$ mice (pink) and WT mice (blue). **C.** Effect of endothelial Cx43 knockout. Leakage in Cx43fl:Tie2-Cre^{POS} animals was somewhat lower compared to Cx43fl:Tie2-Cre^{NEG} controls but the signal did not attain statistical significance. Stars indicate significant elevation above Ctrl (one-sample t-test); number signs indicate significant reduction compared to corresponding controls (Fl/Fl in A; Cre^{NEG} in B & C; two-sample t-test).

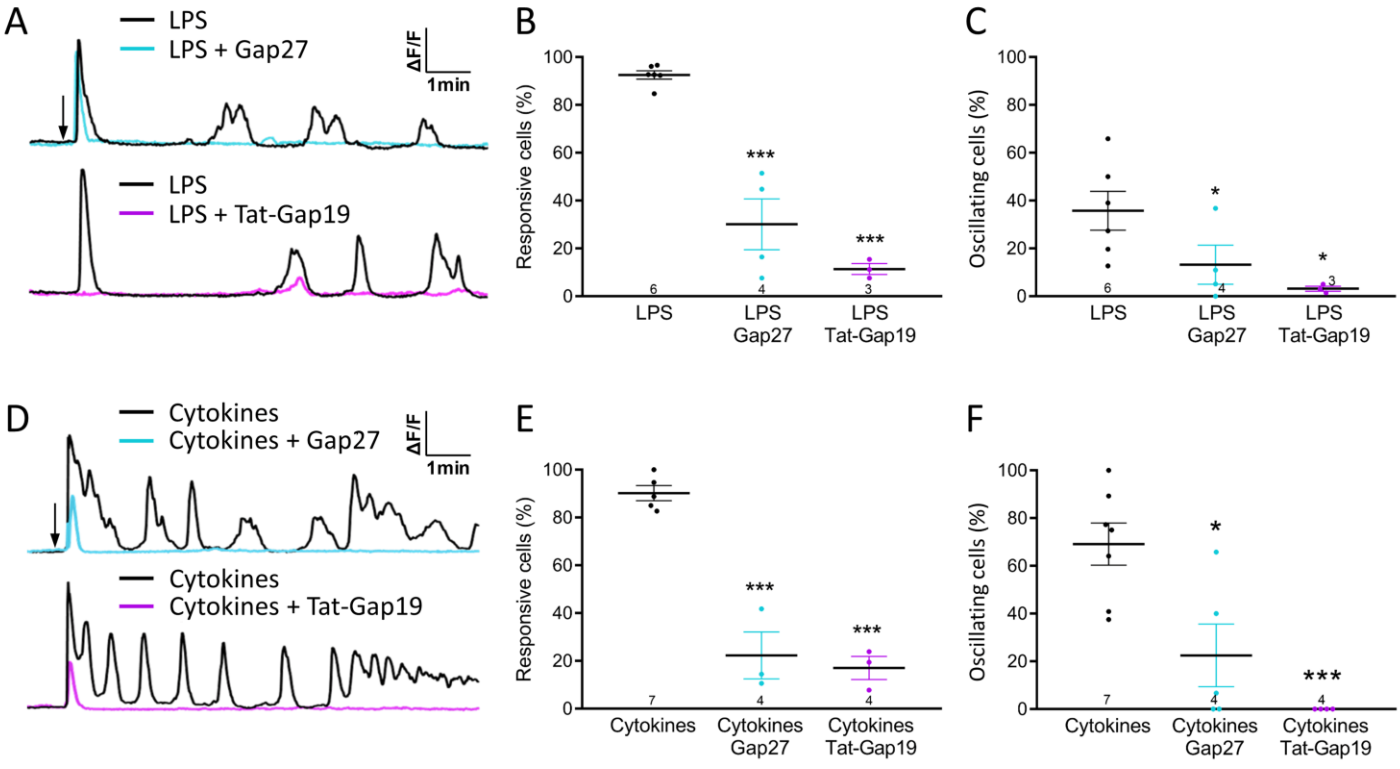

Figure 5. LPS and pro-inflammatory cytokines elicit $[Ca^{2+}]_i$ dynamics in RBE4 cells. A,D. Example traces of $[Ca^{2+}]_i$ dynamics triggered by 1 µg/mL LPS (A) or a mix of pro-inflammatory cytokines (D), and the effect Gap27 or Tat-Gap19 (200 µM, 30 min pre-incubation and present during recording). Arrow marks addition of LPS/cytokines (TNFα, IL1β: 200 pg/mL, IL6: 15 ng/mL, IFNγ: 5 ng/mL as measured in LPS-treated mice). **B-C, E-F.** Percentages of LPS/cytokines-responsive cells (B, E) and oscillating cells (C, F) were significantly reduced by Gap27 and Tat-Gap19. Stars compare to LPS/cytokines mix (one-way ANOVA, Dunnett test).

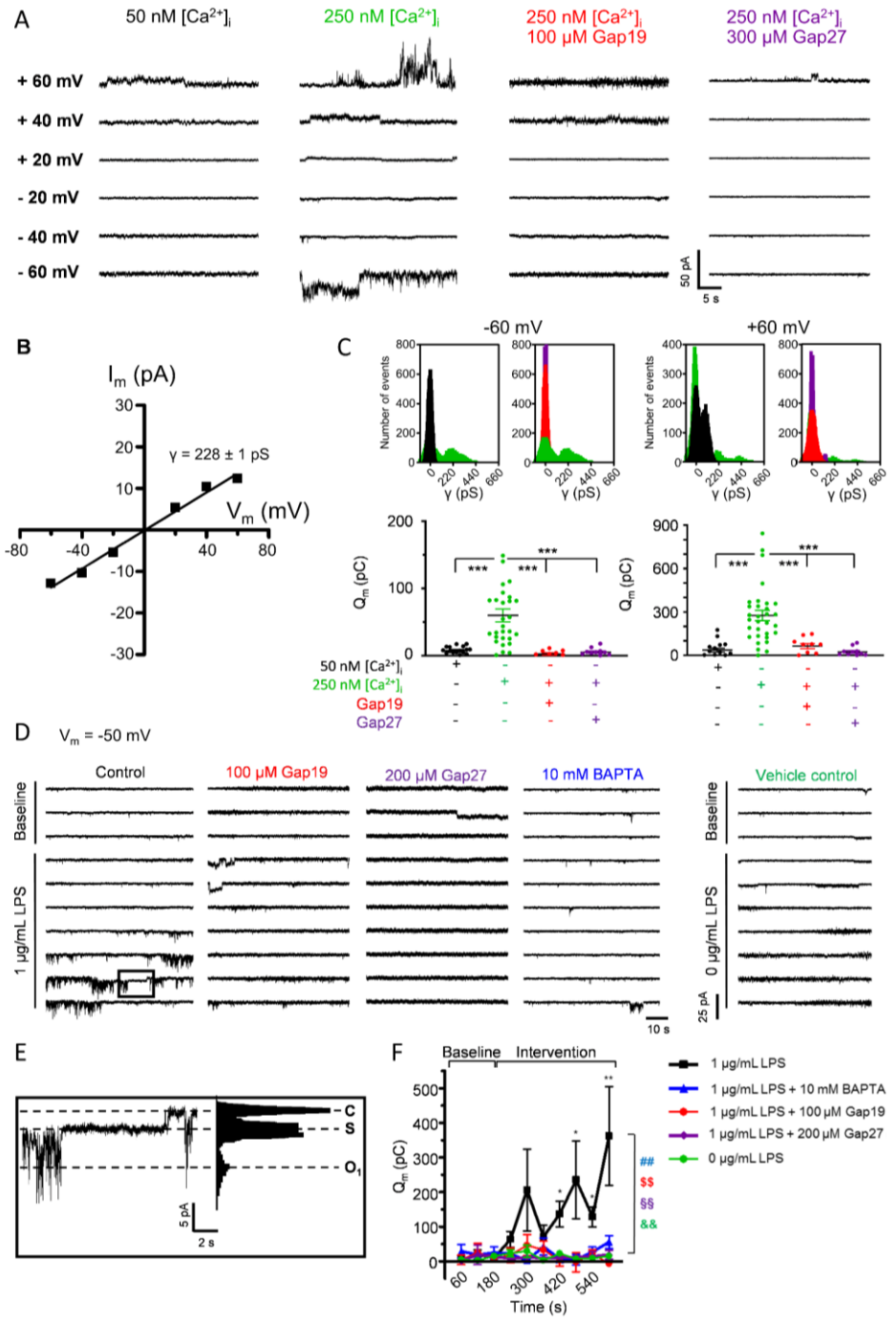

Figure 6. Voltage-, $[Ca^{2+}]_i$- and LPS-dependent activation of Cx43 hemichannels in RBE4 cells. A. Example traces depicting unitary current activities during 30 s voltage steps under conditions of 50 and 250 nM $[Ca^{2+}]_i$. At 250 nM, activity was present at both positive and negative voltages, which was inhibited by Gap19 and Gap27. **B.** I-V plot for 250 nM unitary currents, demonstrating a slope conductance of 228 ± 1 pS (n_{cells} = 48, 5 independent experiments), characteristic for Cx43 hemichannels. **C.** All-point histograms for unitary activities and Q_m summary data at -60 and +60 mV (color codes as in panel A; n_{cells} = 10-31 per condition, 5 independent experiments), showing $[Ca^{2+}]_i$-dependent current activation that is blocked by Gap19 and Gap27 (one-way ANOVA, Bonferroni test). **D-E.** Consecutive current traces obtained at -50 mV (60 s) with and without 1 µg/mL LPS and corresponding all-point histogram (E). LPS induced periodic burst opening of ~210 pS unitary current activity (O_1 in histogram), including a longer lasting substate of ~60 pS (S in histogram). The activity was blocked by Gap19 or 10 mM BAPTA in the patch pipette, or bath-applied Gap27 (30 min pre-incubation). **F.** Q_m summary data of (D) (n_{cells} = 8 per condition; 4 independent experiments). Stars compare LPS time points versus baseline at 60 s (repeated measures ANOVA, Dunnett test). Colored symbols compare LPS to control without LPS (green) and interventions with Gap27 (purple), Gap19 (red) or BAPTA (blue) at the last 600 s time point (one-way ANOVA, Dunnett test).

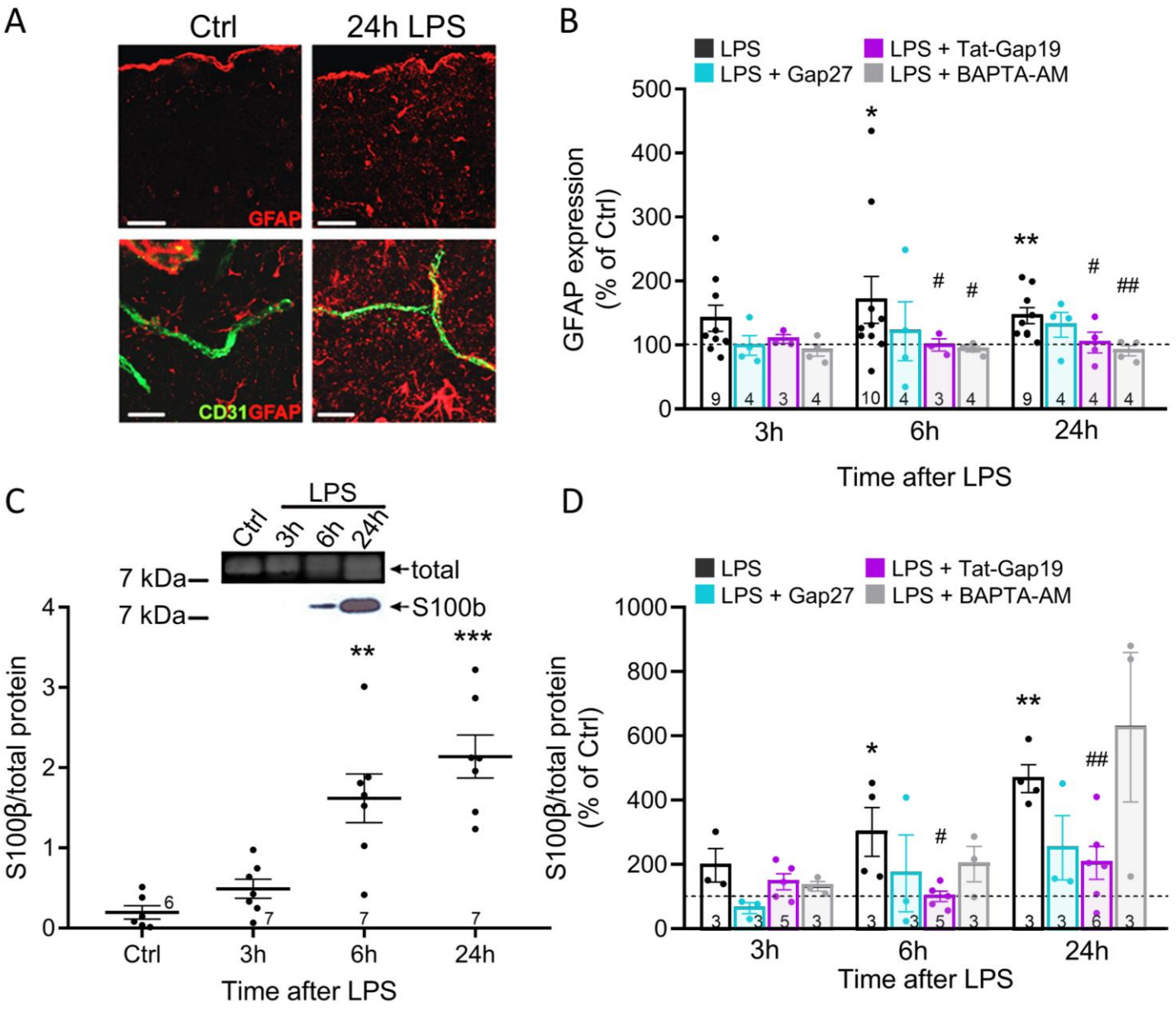

Figure 7. LPS triggers astrogliosis that is inhibited by Tat-Gap19 and BAPTA-AM. A. GFAP immunostaining in the somatosensorial cortex demonstrating LPS-induced astrogliosis. **B.** IV injection of Tat-Gap19 or BAPTA-AM prior to LPS reduced astrogliosis at 6 h and 24 h post-LPS while Gap27 had no effect. Stars indicate significant elevation above Ctrl (one-sample t-test); number signs indicate significant reduction compared to LPS-only (Dunnett test). **C.** The glial inflammation marker S100β appeared in the plasma in response to LPS and was significantly elevated from 6 h on (one-way ANOVA, Dunnett test). **D.** Circulating S100β was reduced by Tat-Gap19, but not by Gap27 or BAPTA-AM (stars, number signs and comparisons as defined in B).

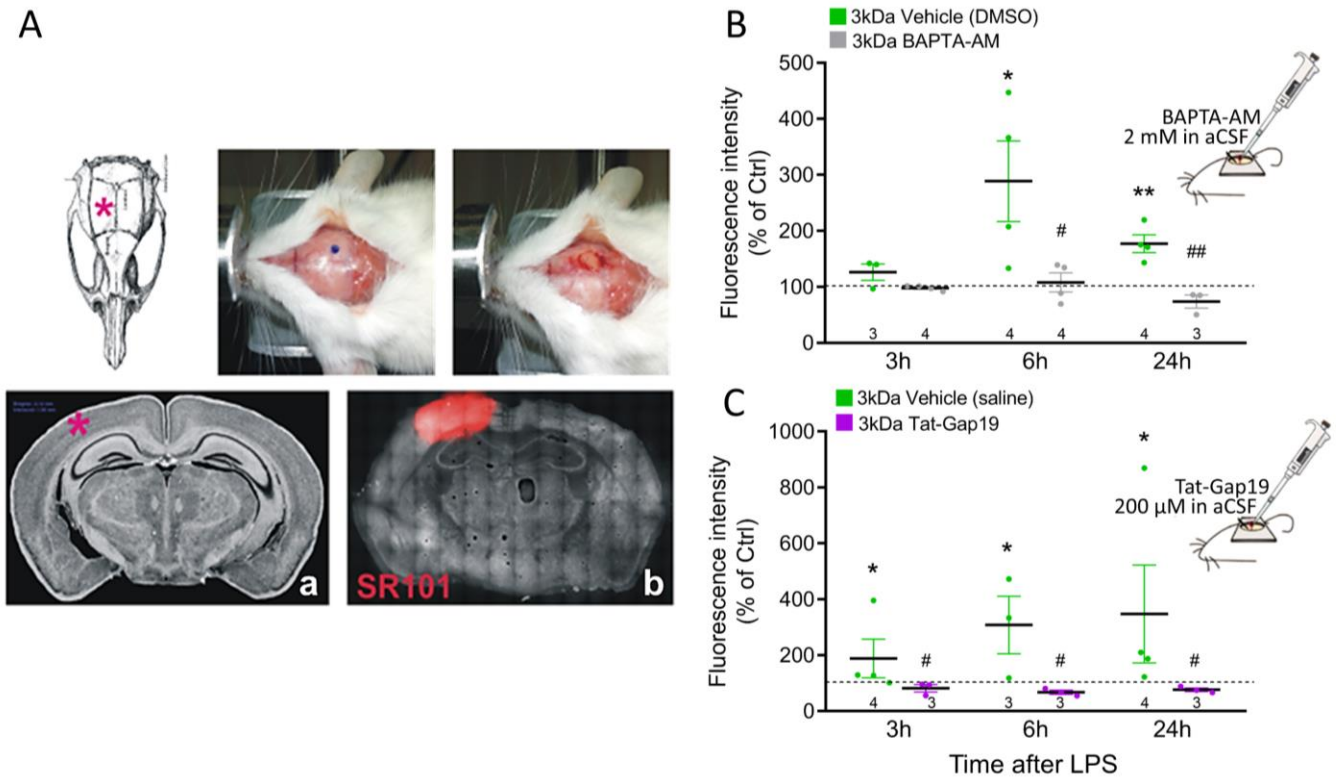

Figure 8. Application of BAPTA-AM or Tat-Gap19 via a cranial window prevents LPS-induced BBB leakage. A. A craniotomy was made in the right parietal bone to create a window (3 mm diameter), centered 2 mm posterior to the bregma and 2 mm from the sagittal suture/midline (red star in skull and image-a below). The loaded zone was visualized by applying SR101 (50 µM) to the exposed cortex and barrier leakage was assessed in this zone only (red zone in image-b). **B-C.** Application of BAPTA-AM or Tat-Gap19 to the exposed cerebral cortex (30 min prior to IP LPS injection) significantly suppressed leakage of 3 kDa DF. Stars compare LPS effect to Ctrl (one-sample t-test); number signs compare intervention (BAPTA-AM, Tat-Gap19) to LPS (vehicle applied to cortex; two-sample t-test).

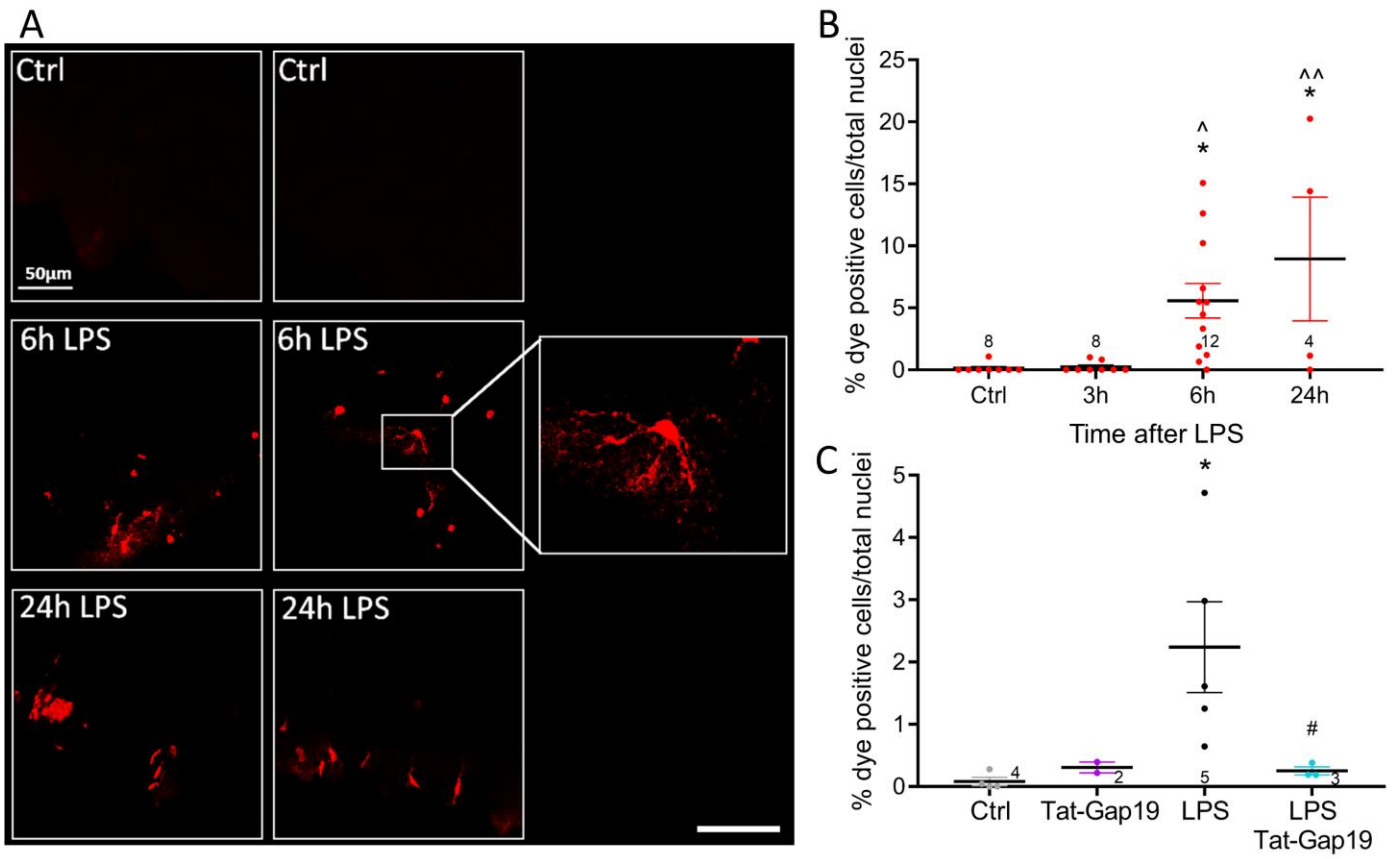

Figure 9. LPS triggers EtBr dye uptake that is inhibited by cortically applied Tat-Gap19. A. Images illustrating cellular EtBr dye uptake after its application to the exposed cortex (100 µM, added 30 min before sarcifice). Scale bar is 20 µm. **B.** The percentage of EtBr dye-positive cells increased with time after IV LPS. Stars compare to Ctrl (one-way ANOVA, Dunnett test). **C.** Effect of Tat-Gap19 (200 µM) at the 6 h post-LPS time point (cortically applied 30 min before EtBr and present with EtBr for the next 30 min). Star compares to Ctrl; number sign compares to LPS without Tat-Gap19 (one-way ANOVA, Bonferroni test).

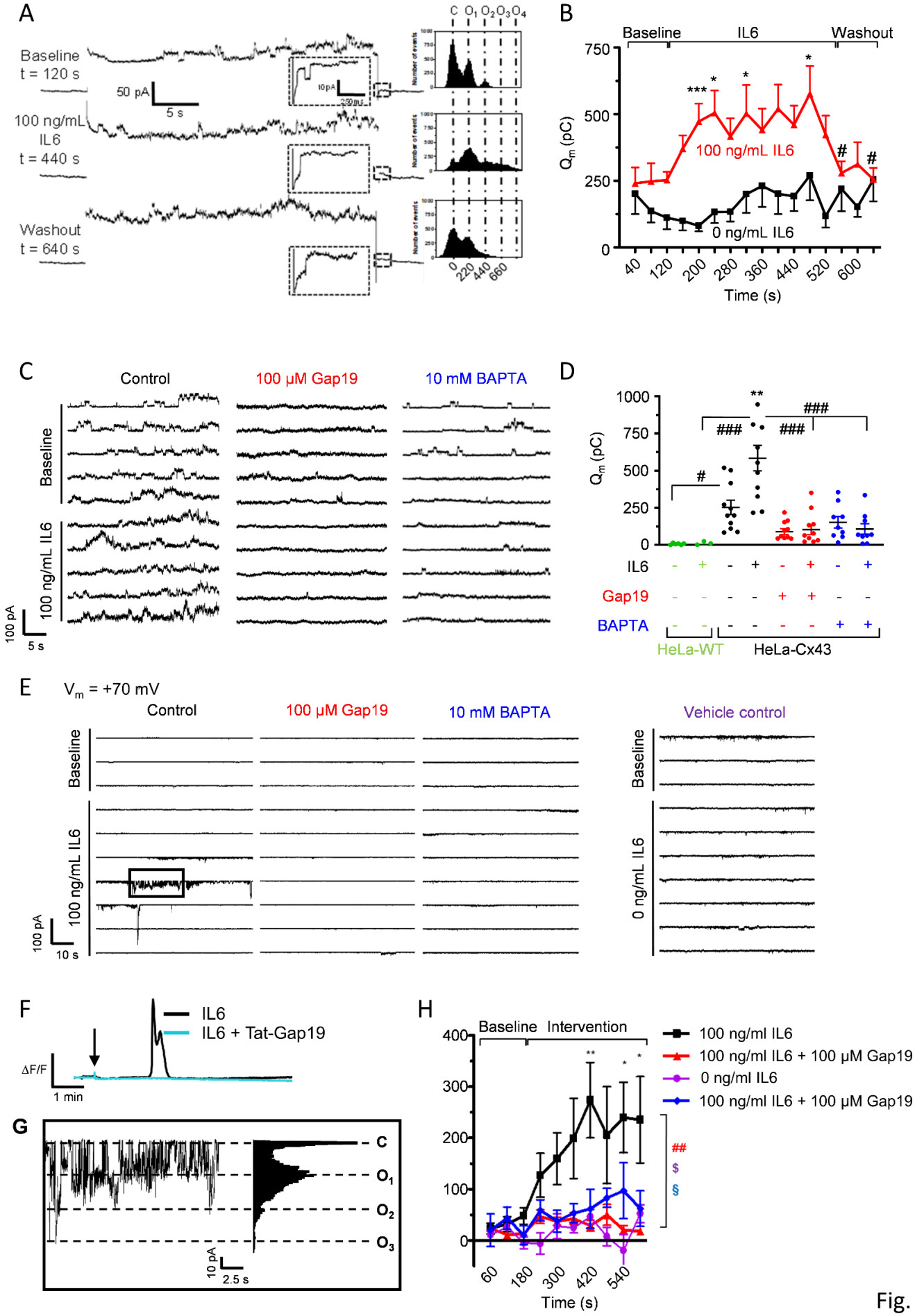
A
Baseline
t = 120 s
50 pA
5 s
100 ng/mL
IL6
t = 440 s
Washout
t = 640 s
C O1 O2 O3 O4
Number of events
0 220 440 660
B
Baseline
IL6
Washout
Qm (pC)
100 ng/mL IL6
0 ng/mL IL6
Time (s)
C
Control
100 µM Gap19
10 mM BAPTA
Baseline
100 ng/mL IL6
100 pA
5 s
D
Qm (pC)
IL6
Gap19
BAPTA
HeLa-WT
HeLa-Cx43
E
Vm = +70 mV
Control
100 µM Gap19
10 mM BAPTA
Vehicle control
Baseline
100 ng/mL IL6
0 ng/mL IL6
100 pA
10 s
F
IL6
IL6 + Tat-Gap19
ΔF/F
1 min
G
C
O1
O2
O3
10 pA
2.5 s
H
Baseline
Intervention
100 ng/ml IL6
100 ng/ml IL6 + 100 µM Gap19
0 ng/ml IL6
100 ng/ml IL6 + 100 µM Gap19
Time (s)

Fig. 10

Figure 10. IL6 enhances Cx43 hemichannel opening in HeLa-Cx43 cells and activates Cx43 hemichannels in primary cultured astrocytes in a Ca^{2+}-dependent manner. A. Example traces and matching all-point histograms depicting representative voltage-induced (+70 mV, 30 s) unitary current activity recorded in HeLa-Cx43 cells before (baseline), during and after application of IL6 (100 ng/mL) via a fast local perfusion system. Insets show hemichannel closing events in the tail currents. **B.** Q_m summary data for repeated current measurements for IL6 (100 ng/mL, red trace) and control (0 µg/mL LPS, black trace) (n_{cells} = 9 per concentration; 5 independent experiments). Red stars compare to 40 s point (repeated measures ANOVA, Dunnett test). Average Q_m during IL6 (160-520 s) was significantly above control without IL6 ($p<0.001$; two-sample t-test). **C.** Representative current traces illustrating the effect of Gap19 and BAPTA applied via the patch pipette. **D.** Q_m summary data of (C) (n_{cells} = 9-11 per condition; 6 independent experiments). Stars compare IL6 versus control without IL6; number signs compare between IL6 and conditions indicated by the lines (one-way ANOVA, Bonferroni test). **E.** Consecutive current traces obtained at -70 mV (60 s) with and without 100 ng/mL IL6 in primary mouse astrocytes. IL6 induced burst unitary current activity that was inhibited by Gap19 or BAPTA added to the patch pipette. **F.** Example traces demonstrating a typical Ca^{2+} response to IL6 (100 ng/mL) in primary astrocytes, which was inhibited by Tat-Gap19 (200 µM, 30 min pre-treatment). **G.** All-point histogram of current activity in the boxed area of (E), demonstrating unitary activity of 220 pS (O_1) and multiples thereof (O_2, O_3). **H.** Q_m summary data of (E) (n_{cells} = 10-17 per condition; 5 independent experiments). Stars compare IL6 time points versus baseline at 120 s (repeated measures ANOVA, Dunnett test). Colored symbols compare IL6 to control without IL6 (purple) and interventions with Gap19 (red) or BAPTA (blue) at the last 600 s time point (one-way ANOVA, Dunnett test).

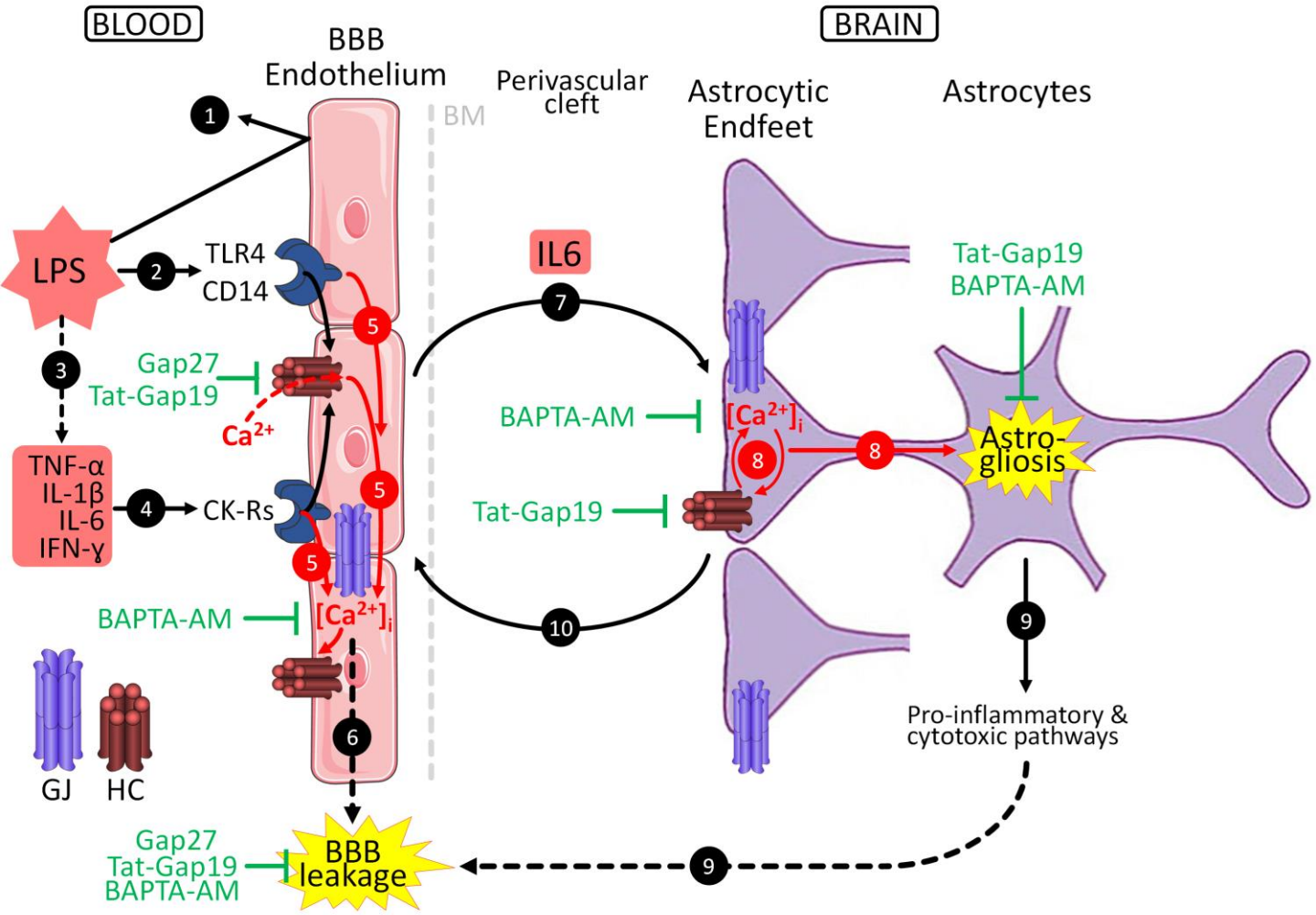

Figure 11. Schematic drawing summarizing the findings of this study. Numbered steps are explained in the Discussion. The perivascular cleft has been stretched for clarity. BM, basement membrane.